Computation and Graphic Characterization of Robust Multiple-Contact Postures in Gravitational Environments

Yizhar Or and Elon Rimon
Dept. of Mechanical Engineering, Technion, Israel
izi@tx.technion.ac.il, rimon@tx.technion.ac.il
Technical Report, June 2004

Abstract *This paper is concerned with the problem of identifying robust equilibrium postures of a planar mechanism supported by multiple frictional contacts in a two-dimensional gravitational field. The complex kinematic structure of the mechanism is lumped into a single rigid body, $\mathcal{B}$, with a variable center of mass. Inertial forces generated by moving parts of the mechanism are lumped into a neighborhood of wrenches centered at the nominal gravitational wrench. The identification of the robust equilibrium postures associated with a given set of contacts is reduced to the identification of center-of-mass locations that maintain equilibrium of $\mathcal{B}$ with respect to any wrench in the given neighborhood. The static response of $\mathcal{B}$ to an external wrench involves static indeterminacy and frictional constraints. The region of center-of-mass locations that generate equilibrium with respect to a particular external wrench is formulated as a linear programming problem, and a full graphic characterization is provided. Next, the results are then generalized to a neighborhood of external wrenches, and to the situation of distributed contact patches. Then we present experimental results that validate the analytical criterion of feasible equilibrium. Finally, we present first steps towards computing feasible equilibrium postures in 3D.*

1 Introduction

Multi-legged locomotion in a gravitational environment requires criteria for identifying and computing feasible equilibrium postures. This paper is concerned with the problem of identifying and computing the feasible equilibrium postures of a multi-limbed mechanism supported by multiple frictional contacts in a two-dimensional gravitational field. In order to simplify the problem, we lump the complex kinematic structure of the mechanism into a single rigid body, $\mathcal{B}$, with a variable center of mass. Since free limbs of the mechanism must move during locomotion, we lump the inertial forces generated by its moving parts into a neighborhood of disturbance wrenches (i.e. forces and torques) centered at the nominal gravitational wrench. We seek for equilibrium postures which are robust, in the sense that they maintain equilibrium for any external wrench within the given neighborhood. The identification of the feasible equilibrium postures associated with a given set of contacts and a given external wrench is reduced to the identification of center-of-mass locations that

generate feasible equilibrium of $\mathcal{B}$, while satisfying the friction constraints at the contacts. However, in our case $\mathcal{B}$ is subjected to a neighborhood of external wrenches rather than a single wrench. Hence we introduce the notion of *robust equilibrium.* By definition, $\mathcal{B}$ is in a robust equilibrium with respect to a neighborhood of wrenches if it maintains feasible equilibrium with respect to all wrenches in the neighborhood. In other words, the contacts supporting the object can statically resist the entire neighborhood of wrenches that can act on $\mathcal{B}$. Based on this notion of robustness, our objective is as follows. Given a set of contacts and a neighborhood of wrenches centered at the nominal gravitational wrench, we wish to identify all center-of-mass locations guaranteing a robust equilibrium posture of $\mathcal{B}$.

Our paper makes three contributions toward this objective. First, we formulate the conditions for a multiple-contact feasible equilibrium posture as a linear programming problem in terms of $\mathcal{B}$'s center-of-mass location, for a single external wrench and for a given neighborhood of wrenches. Second, we provide a full graphic characterization for multiple-contact feasible equilibrium postures. Third, we generalize the results for distributed contact patches.

Many Researches have been conducted on legged locomotion. Madhani and Dubowsky [13] developed a locomotion planner in the full configuration space using nonlinear optimization over discrete nodes, considering friction constraints and static indeterminacy. Boissonnat et. al. [2] presented an algorithm for legged robots motion planning avoiding obstacles, without consideration of friction and static response at contacts. These methods are based on the full configuration space of the robot, and hence are computationally intensive. Working with frictionless contacts, Mason et al. [15] introduced the idea of lumping the kinematic structure of a mechanism into a rigid body having the same contacts with the environment and a variable center of mass. They identified the statically stable postures of a mechanism supported by *frictionless* contacts in two and three-dimensions. A similar work has been conducted by Trinkle et al. [22, 23] in the context of whole-arm manipulation, and by Kriegman [10] in the context of object recognition. However, stability in a *frictional* gravitational environment requires a consideration the associated dynamics, which is not governed by any obvious potential energy. Several researchers considered the role of compliance in frictionless grasp stability, e.g. [11, 8]. Other researchers attempted to analyze grasp stability based on compliance introduced by stiffness-control laws (e.g. [1, 7, 24]). However, the mechanics of compliance at a frictional contact is still being investigated in the solid mechanics literature [9]. Our objective is to characterize stable postures under the simplification of rigid body paradigm, assuming that the contact forces are passive, and cannot be sensed or controlled. A key problem, is that the rigid body dynamics with frictional contacts can be ambiguous [12, 14], and the dynamic analysis must include all the possible contact modes [21, 5]. Our approach divides into two stages [18]. The first stage, presented in this paper, is to efficiently identify the feasible equilibrium postures. The second stage is dynamic analysis, where we use the criterion of *strong stability* defined by Trinkle et. al. [20]. This work will be presented in a paper currently under preperation. Bretl and Latombe [3] analyze the feasible center-of-mass positions for a robot climbing on vertical walls with frictional supports. Erdmann et. al. [6] characterize the feasible center-of-mass positions for two frictional contacts in the context of nonprehensile palm manipulation. However, no previous work have explicitly formulated the feasible positions for a general number of contacts, or considered robustness with respect to a neighborhood of external disturbances presented here.

The structure of the paper is as follows. In the next section we formulate the equilibrium

condition and frictional constraints, compute the feasible equilibrium region for multiple contacts by solving a linear programming problem, and provide a graphic characterization of this region. In section 3 we generalize for a neighborhood of disturbance wrenches and compute the robust equilibrium region. In section 4 we generalize for the case of distributed contact patches instead of contact points. In section 5, we present preliminary experimental results of a two-contact posture under disturbance wrenches, that validate the analytical criterion of feasible equilibrium. In section 6, we present first steps towards computing feasible equilibrium postures in 3D. Finally, the concluding section describes the need to account for dynamic ambiguity associated with Coulomb's friction model.

2 The Feasible Equilibrium Region

Given a planar body $\mathcal{B}$ with variable center-of-mass supported by k contacts against gravity, the *feasible equilibrium region* consists of the center-of-mass locations that can generate an equilibrium posture of $\mathcal{B}$. In this section we characterize the feasible equilibrium region under the following assumptions. First, the terrain is assumed to be *piecewise linear*. Second, we assume that $\mathcal{B}$ as well the supporting contacts are ideally rigid, and each support makes a point contact with $\mathcal{B}$. The latter assumption is relaxed below, where we generalize the results to contact patches. Third, we assume that the contact points are known.

2.1 Basic Terminology

Let $x_1 \dots x_k$ denote the stationary contact points supporting $\mathcal{B}$, expressed with resect to a fixed world frame. Let x denotes $\mathcal{B}$'s center of mass. The forces acting on $\mathcal{B}$ at the contacts are denoted $f_1 \dots f_k$, and described with respect to the fixed world frame. The torque generated by f_i about $\mathcal{B}$'s center of mass is given by the scalar $\tau_i = (x_i - x)^T J^T f_i$, where $J = \begin{bmatrix} 0 & -1 \\ 1 & 0 \end{bmatrix}$. The gravitational force acting on $\mathcal{B}$ is denoted f_g. We also allow a disturbance wrench (f_d, τ_d) acting on $\mathcal{B}$'s center-of-mass. Let $\boldsymbol{w} = (f_{ext}, \tau_{ext}) \in I\!R^2 \times I\!R$ denote the net external wrench acting on $\mathcal{B}$'s center-of-mass. Then $f_{ext} = f_g + f_d$ such that $\|f_d\| \ll \|f_g\|$. Since f_g generates no torque about x, we have that $\tau_{ext} = \tau_d$. Finally, t_i and n_i denote unit vectors in the tangential and normal directions at x_i respectively, such that n_i is pointing away from the terrain and $n_i = Jt_i$. We assume that t_i, n_i and x_i for $i = 1 \dots k$ are known.

When an external wrench $\boldsymbol{w}$ acts on $\mathcal{B}$, the equilibrium condition is:

$$\begin{aligned} f_1 + \cdots + f_k &= -f_{ext} \\ (x_1 - x)^T J^T f_1 + \cdots + (x_k - x)^T J^T f_k &= -\tau_{ext} \end{aligned} \tag{1}$$

Note that the contact forces are statically indeterminate for $k \geq 2$ contacts. Furthermore, the Coulomb friction law states that each force f_i must lie in a *friction cone,* denoted $\mathcal{C}_i$, in order to avoid sliding. Let μ be the coefficient of friction, and let f_i^n and f_i^t denote the normal and tangential components of f_i. Then $\mathcal{C}_i = \{f_i : |f_i^t| \leq \mu f_i^n,\ f_i^n \geq 0\}$. We also need the following equivalent terminology for $\mathcal{C}_i$. Let C_i^u and C_i^w denote unit vectors along the two edges of $\mathcal{C}_i$ (Figure 1(a)). Then the i^{th} friction cone is given by $\mathcal{C}_i = \{f_i^u C_i^u + f_i^w C_i^w : f_i^u, f_i^w \geq 0\}$. The *feasible equilibrium region*, denoted $\mathcal{R}(\boldsymbol{w})$, is the set of center-of-mass locations, x, for which

there exist feasible contact forces $f_i \in \mathcal{C}_i$ $(i = 1 \ldots k)$ that satisfy the equilibrium condition (1).

2.2 Computation of the Feasible Equilibrium Region

We now show that the feasible equilibrium region $\mathcal{R}(\boldsymbol{w})$ where $\boldsymbol{w} = (f_{ext}\,, \tau_{ext}\,)$ is an infinite strip parallel to f_{ext} , which can be computed as a linear programming problem. Each contact force can be written as $f_i = C_i^u f_i^u + C_i^w f_i^w$ where $f_i^u, f_i^w \geq 0$ and C_i^u, C_i^w are the edges of $\mathcal{C}_i$. First we write the equilibrium condition(1). using the following rasp matrix terminology [17]. Let us define:

$$G_f = \left[\begin{array}{cccccc} C_1^u & C_1^w & \cdots & C_k^u & C_k^w \end{array}\right]_{2\times 2k}$$

$$G_\tau = \left[\begin{array}{cccccc} x_1^T J^T C_1^u & x_1^T J^T C_1^w & \cdots & x_k^T J^T C_k^u & x_k^T J^T C_k^w \end{array}\right]_{1\times 2k}$$

$$\vec{f} = \begin{pmatrix} f_1^u \\ f_1^w \\ \vdots \\ f_k^u \\ f_k^w \end{pmatrix}_{2k\times 1}.$$

Then the equilibrium equation (1) can be written as follows:

$$\left[\begin{array}{c} G_f \\ G_\tau \end{array}\right] \vec{f} = -\begin{pmatrix} f_{ext} \\ \tau(x) \end{pmatrix} \text{ and } \vec{f} \geq \vec{0}, \tag{2}$$

where $\tau(x) = x^T J^T f_{ext} + \tau_{ext}$ is the net torque generated by $\boldsymbol{w}$ about the world frame origin. Notice that x is eliminated from the left hand side of (2). The following key Theorem characterizes the feasible equilibrium region of $\boldsymbol{w}$ as a linear programming problem.

Theorem 1. *Let $\mathcal{B}$ be supported by k frictional contacts in a two-dimensional gravitational field, and be subjected to an external wrench $\boldsymbol{w} = (f_{ext}\,, \tau_{ext}\,)$. Then the feasible equilibrium region $\mathcal{R}(\boldsymbol{w})$ is the **infinite strip** given by*

$$\mathcal{R}(\boldsymbol{w}) = \big\{x : \tau_{min} \leq x^T J^T f_{ext} + \tau_{ext} \leq \tau_{max}\big\}, \tag{3}$$

where τ_{min} and τ_{max} are obtained by solving the linear programming problems:

$$\tau_{min} = \min_{G_f \vec{f} = -f_{ext}\ ,\, \vec{f} \geq \vec{0}} \{-G_\tau \vec{f}\} \qquad \tau_{max} = \max_{G_f \vec{f} = -f_{ext}\ ,\, \vec{f} \geq \vec{0}} \{-G_\tau \vec{f}\} \tag{4}$$

Intuitively, $G_\tau \vec{f}$ is the net torque generated by the contacts in response to $\boldsymbol{w}$. The interval $[\tau_{min}, \tau_{max}]$ captures the range of torques that can be resisted by the contacts. Hence any center-of-mass location satisfying $\tau_{min} \leq \tau(x) \leq \tau_{max}$ allows the contacts to balance the net wrench acting on $\mathcal{B}$.

Proof: Let $\vec{f}_{min}$ and $\vec{f}_{max}$ denote the values of $\vec{f}$ corresponding to the extreme values τ_{min} and τ_{max} in (4). Any $\tau(x) \in [\tau_{min}, \tau_{max}]$ can be expressed as $\tau(x) = \lambda\tau_{min} + (1-\lambda)\tau_{max}$ where $\lambda \in [0, 1]$. Taking $\vec{f} = \lambda\vec{f}_{min} + (1-\lambda)\vec{f}_{max}$, one gets

$$\begin{aligned} &G_f \vec{f} = \lambda G_f \vec{f}_{min} + (1-\lambda) G_f \vec{f}_{max} = -f_{ext} \\ &G_\tau \vec{f} = \lambda G_\tau \vec{f}_{min} + (1-\lambda) G_\tau \vec{f}_{max} = -\lambda\tau_{min} - (1-\lambda)\tau_{max} = -\tau(x) \\ &\vec{f} = \lambda\vec{f}_{min} + (1-\lambda)\vec{f}_{max} \geq \vec{0}. \end{aligned}$$

Hence for any external torque $\tau(x) \in [\tau_{min}, \tau_{max}]$, there exist contact forces $\vec{f}$ that satisfy the equilibrium condition (2). It follows that the strip $\tau_{min} \leq \tau(x) \leq \tau_{max}$ defines the feasible equilibrium region $\mathcal{R}(\boldsymbol{w})$. □

Example 1: Figure 1(a) shows an example of $\mathcal{R}(\boldsymbol{w})$ for two contacts using the nominal gravitational wrench $\boldsymbol{w} = (f_g, 0)$. Note that in this case $\mathcal{R}(\boldsymbol{w})$ is the vertical strip spanned by the polygon $\mathcal{C}_1 \cap \mathcal{C}_2$. The physical justification for this fact is discussed below.

2.3 Structural Properties of the Feasible Equilibrium Region

We now describe two significant structural properties of $\mathcal{R}(\boldsymbol{w})$. The first property will prove to be extremely useful in the ensuing graphic characterization of $\mathcal{R}(\boldsymbol{w})$, and is stated in the following proposition.

Proposition 2.1. *Let $\mathcal{B}$ be supported by k frictional contacts in a two-dimensional gravitational field, and be subjected to an external wrench $\boldsymbol{w} = (f_{ext}, \tau_{ext})$. Then $\mathcal{R}(\boldsymbol{w})$ is the convex hull of the pairwise feasible equilibrium regions,*

$$\mathcal{R}(\boldsymbol{w}) = \mathsf{conv}\{\mathcal{R}_{ij}(\boldsymbol{w}) \ , \ 1 \leq i, j \leq k\}$$

where $\mathcal{R}_{ij}(\boldsymbol{w})$ is the feasible equilibrium region associated with the two contacts x_i and x_j, and conv *denotes convex hull.*

The proposition implies that when constructing $\mathcal{R}(\boldsymbol{w})$ for multiple-contact postures, one simply needs to consider the feasible equilibrium strips generated by all pairs of contacts. Taking the convex hull of these parallel strips can be performed by simply identifying their leftmost and rightmost edges.

Proof: Let us denote $\mathcal{R} = \mathsf{conv}\{\mathcal{R}_{ij}(\boldsymbol{w}) \ , \ 1 \leq i, j \leq k\}$, where conv denotes convex hull. The proof is divided into two steps. First we show that $\mathcal{R} \subseteq \mathcal{R}(\boldsymbol{w})$, and then we show that $\mathcal{R}(\boldsymbol{w}) \subseteq \mathcal{R}$.

1. Assume that $x \in \mathcal{R}$. From the definition of convex hull, there exist center-of-mass locations $x_{ij} \in \mathcal{R}_{ij}(\boldsymbol{w})$ and non-negative coefficients λ_{ij} such that $\sum_{i,j} \lambda_{ij} x_{ij} = x$ where $\sum_{i,j} \lambda_{ij} = 1$. Consider now only the (i, j) indices such that $\lambda_{ij} \neq 0$. Since $x_{ij} \in \mathcal{R}_{ij}(\boldsymbol{w})$, there exists a $2k$-vector $\vec{f}_{ij} \geq \vec{0}$ in which the only non-zero components are the ones associated with the contact forces at x_i and x_j, that satisfies the equilibrium condition $G_f \vec{f}_{ij} = -f_{ext}$ and $G_\tau \vec{f}_{ij} = -(x_{ij}^T J^T f_{ext} + \tau_{ext})$. If one now chooses a vector of contact forces $\vec{f} = \sum_{i,j} \lambda_{ij} \vec{f}_{ij} \geq \vec{0}$, one gets

   $$G_f \vec{f} = \sum_{i,j} \lambda_{ij} G_f \vec{f}_{ij} = -\sum_{i,j} \lambda_{ij} f_{ext} = -f_{ext}$$
   $$G_\tau \vec{f} = \sum_{i,j} \lambda_{ij} G_\tau \vec{f}_{ij} = -\sum_{i,j} \lambda_{ij} (x_{ij}^T J^T f_{ext} + \tau_{ext}) = -(x^T J^T f_{ext} + \tau_{ext})$$

   Thus $\vec{f}$ satisfies the equilibrium condition (2) with center-of-mass at x, and hence $x \in \mathcal{R}(\boldsymbol{w})$.

2. Assume that $x \in \mathcal{R}(\boldsymbol{w})$. Let τ_{min} and τ_{max} be the solutions of the LP problems (4), computed for the given wrench $\boldsymbol{w}$. Let $\vec{f}_{min}$ and $\vec{f}_{max}$ be the values of $\vec{f}$ corresponding

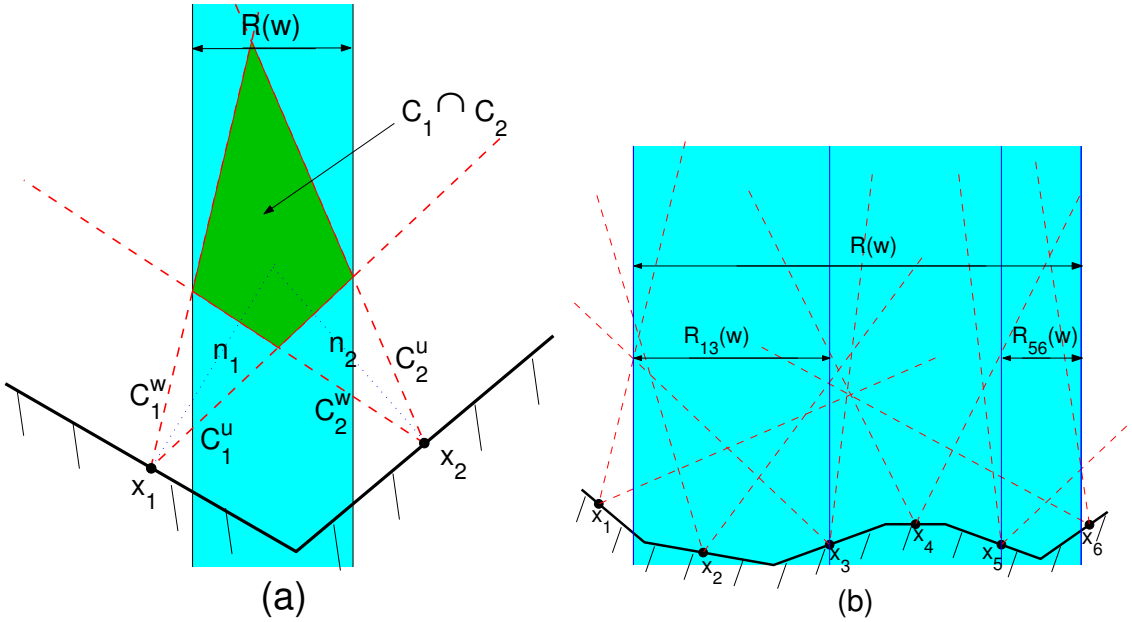

Figure 1: Computation of $\mathcal{R}(\boldsymbol{w})$ for (a) two contacts and (b) six contacts.

to τ_{min} and τ_{max}. Since x lies in the strip $\mathcal{R}(\boldsymbol{w}) = \{x : \ \tau_{min} \leq x \cdot J^T f_{ext} + \tau_{ext} \leq \tau_{max}\}$, there exist two points x_{min} and x_{max} lying on the edges of $\mathcal{R}(\boldsymbol{w})$, such that $x = \lambda x_{min} + (1-\lambda) x_{max}$ for some $\lambda \in [0,1]$.

Now recall that the extrema of a linear programming problem always include a vertex of the polytope defined by the problem's constraints [4]. (Even when the extremum occurs on an edge, there exists at least one vertex at which the extremum is attained). Let $\mathcal{P}$ denote the polytope defined by the constraints of (4), $\mathcal{P} = \{\vec{f} \in I\!R^{2k} : \ G_f \vec{f} = -f_{ext}\,, \vec{f} \geq \vec{0}\}$. We can see that $\mathcal{P}$ is defined by two equalities and $2k$ inequalities in $I\!R^{2k}$. A vertex of $\mathcal{P}$ is an intersection point of $2k$ facets of $\mathcal{P}$. Hence a vertex point, denoted $\vec{f}_v$, satisfies $2k$ equalities out of the $2k+2$ equations $\{\vec{f}_v = \vec{0}\,,\ G_f \vec{f}_v = -f_{ext}\,\}$. As a result, $\vec{f}_v$ has no more than two non-zero components. Since τ_{min} is an extremum value of (4), $\vec{f}_{min}$ is a vertex of $\mathcal{P}$ and hence has no more than two non-zero components. Hence there exist two indices i and j such that $\vec{f}_{min}$ corresponds to contact forces generated only at x_i and x_j. But $\vec{f}_{min}$ corresponds to x_{min}, and hence satisfies $G_f \vec{f}_{min} = -f_{ext}$ and $G_\tau \vec{f}_{min} = -\tau_{min} = -(x_{min}^T J^T f_{ext} + \tau_{ext}\,)$. Since $\vec{f}_{min}$ corresponds to contact forces only at x_i and x_j and satisfies the equilibrium condition (2) with $x = x_{min}$, we conclude that $x_{min} \in \mathcal{R}_{ij}(\boldsymbol{w})$. Using similar arguments for $\vec{f}_{max}$, we can conclude that there exist two indices m and n such that $x_{max} \in \mathcal{R}_{mn}$. Recalling that $x = \lambda x_{min} + (1-\lambda) x_{max}$, we conclude that $x \in conv\{\mathcal{R}_{ij}(\boldsymbol{w}), \mathcal{R}_{mn}\} \subseteq \mathcal{R}$ $\square$

The second observation is that the frictional contacts can be classified into essential and redundant contacts, as follows. Any $x \in \mathcal{R}(\boldsymbol{w})$ can be balanced using the essential contacts only, while the redundant contacts can be removed. Furthermore, for any posture there are no more than *four* essential contacts. This observation is stated in the following corollary.

Corollary 2.2. *Let $\mathcal{B}$ be supported by $k \geq 4$ frictional contacts in a two-dimensional gravitational field, and be subjected to an external wrench $\boldsymbol{w} = (f_{ext}\,, \tau_{ext}\,)$. Let $\mathcal{R}(\boldsymbol{w})$ be the*

feasible equilibrium region associated with $\boldsymbol{w}$. *Then there exist at least* $k-4$ *contacts that can be removed without affecting* $\mathcal{R}(\boldsymbol{w})$.

Notice that the particular partition of essential and redundant contacts depends only on the contacts arrangement and is independent of the center-of-mass location.

Proof: The proof is based on the proof of proposition 2.1 . Following the arguments of step 2, there exist at most four distinct contacts x_i, x_j, x_m, x_n such that $\mathcal{R}(\boldsymbol{w}) = conv\{\mathcal{R}_{ij}(\boldsymbol{w}), \mathcal{R}_{mn}\}$. Therefore, by using the arguments of step 1, we can conclude that for any $x \in \mathcal{R}(\boldsymbol{w})$, the external wrench $\boldsymbol{w}$ can be supported by reaction forces at these four contacts only. □

Example 2: Figure 1(b) shows an example of $\mathcal{R}(\boldsymbol{w})$ for a six-contacts posture using the nominal gravitational wrench $\boldsymbol{w} = (f_g, 0)$. Computing the vertical strips $\mathcal{R}_{ij}(\boldsymbol{w})$ associated with all the possible pairs of contacts, one can see that the leftmost edge is associated with $\mathcal{R}_{13}$, and the rightmost edge is associated with $\mathcal{R}_{56}$. Therefore, the contacts x_1, x_3, x_5 and x_6 are essential contacts, and the contacts x_2 and x_4 are redundant, and can be removed without reducing $\mathcal{R}(\boldsymbol{w})$. We must emphasize here that x_2 and x_4 are redundant only for the construction of $\mathcal{R}(\boldsymbol{w})$, but may be necessary for some other considerations such as minimizing contact forces, or guaranteeing dynamic stability, which are out of this paper's scope.

2.4 Graphic Characterization of $\mathcal{R}(\boldsymbol{w})$

We now present a graphic characterization of the feasible equilibrium region $\mathcal{R}(\boldsymbol{w})$. Recall that $\mathcal{R}(\boldsymbol{w})$ for a k-contact posture can be obtained by first constructing the feasible equilibrium strips for all pairs of contacts, then taking the convex hull of these strips. Therefore, we now focus on the case of two-contact postures. We start with the nominal gravitational wrench $\boldsymbol{w}_o = (f_g, 0)$. The region $\mathcal{R}(\boldsymbol{w}_o)$ is a vertical strip that can be obtained by union and intersection of *five* strips, each having a distinct graphic interpretation. Before stating the procedure for constructing $\mathcal{R}(\boldsymbol{w}_o)$, we need the following notation. Recall that $\mathcal{C}_i$ denotes the friction cone at x_i. Let $\mathcal{C}_i^-$ denote the negative reflection of $\mathcal{C}_i$ about x_i. Next, let S_1^{++} denote the infinite vertical strip spanned by the polygon $\mathcal{C}_1 \cap \mathcal{C}_2$. Similarly, let S_1^{+-}, S_1^{-+}, and S_1^{--} denote the infinite vertical strips spanned by the polygons $\mathcal{C}_1^+ \cap \mathcal{C}_2^-$, $\mathcal{C}_1^- \cap \mathcal{C}_2^+$, and $\mathcal{C}_1^- \cap \mathcal{C}_2^-$ respectively. Note that some of these polygons and their associated strips may be empty. Finally, let S_2 denote the infinite vertical strip bounded by the contacts x_1 and x_2. The procedure for constructing $\mathcal{R}(\boldsymbol{w}_o)$ is summarized in the following lemma.

Lemma 2.3. *Let* $\mathcal{B}$ *be supported by two frictional contacts in a two-dimensional gravitational field, and be subjected the gravitational wrench* $\boldsymbol{w}_o = (f_g, 0)$. *Then the feasible equilibrium region* $\mathcal{R}(\boldsymbol{w}_o)$ *is the infinite vertical strip given by*

$$\mathcal{R}(\boldsymbol{w}_o) = \big((S_1^{++} \cup S_1^{--}) \cap S_2\big) \cup \big((S_1^{+-} \cup S_1^{-+}) \cap \bar{S}_2\big),$$

where $\bar{S}_2$ *is the complement of* S_2 *in* $I\!R^2$.

Proof: Recall the equilibrium condition (1). There are three external forces acting on $\mathcal{B}$: the gravitational force f_g at x, and the contact forces f_1 and f_2 at x_1 and x_2. The balance of moments implies that the three force lines must intersect at a single point, denoted

z. (In the special case where all forces are parallel, z is located at infinity). Since the contact force f_i must lie in its friction cone $\mathcal{C}_i$, z must lie within the double-cone $\mathcal{C}_i \cup \mathcal{C}_i^-$ for $i = 1, 2$. Since the vertical line of f_g passes through z and x, we conclude that in order to generate an equilibrium solution, x must lie within one of the infinite vertical strips spanned by $(\mathcal{C}_1 \cup \mathcal{C}_1^-) \cap (\mathcal{C}_2 \cup \mathcal{C}_2^-)$, which are precisely $S_1^{++}, S_1^{+-}, S_1^{-+}$ and S_1^{--} (Figure 1(a)-(b)) .However, this observation does not capture the condition that the contact forces can only push on the object, $f_i^n \geq 0$ for $i = 1, 2$. For example, in Figure 2(c) the polygon $\mathcal{C}_1 \cap \mathcal{C}_2$ is semi-infinite, and S_1^{++} is consequently a halfplane, and some equilibrium contact forces have negative normal components. We now derive an additional graphic condition which is equivalent to the requirement $f_i^n \geq 0$. Let u_i denote the unit vector pointing from x_i to z for $i = 1, 2$. First we assume that the forces' intersection point satisfies $z \in \mathcal{C}_1 \cap \mathcal{C}_2$, and thus $u_i \in \mathcal{C}_i$ for $i = 1, 2$. Then f_i can be written as $f_i = \alpha_i u_i$ such that $\alpha_i \geq 0$ for $i = 1, 2$. Let $f_g^\perp = J f_g$ denote the horizontal direction. Taking the force balance $f_1 + f_2 = -f_g$ and projecting it onto $f_g^\perp$, gives $\alpha_1(u_1 \cdot f_g^\perp) + \alpha_2(u_2 \cdot f_g^\perp) = 0$. Since $\alpha_i \geq 0$, we conclude that the terms $u_1 \cdot f_g^\perp$ and $u_2 \cdot f_g^\perp$ must have opposite signs. The graphical interpretation of this fact is that z must lie inside the vertical strip bounded by the contacts, denoted S_2. Since x and z lie on the same vertical line, x must lie in the intersection $S_1^{++} \cap S_2$ (Figure 1(c)).
Second, if the forces' intersection point satisfies $z \in \mathcal{C}_1 \cap \mathcal{C}_2^-$, we have $u_1 \in \mathcal{C}_1$, and $u_2 \in \mathcal{C}_2^-$. Hence f_i are written as $f_i = \alpha_i u_i$ such that $\alpha_1 \geq 0$ and $\alpha_2 \leq 0$. Therefore, the horizontal force balance $\alpha_1(u_1 \cdot f_g^\perp) + \alpha_2(u_2 \cdot f_g^\perp) = 0$ now implies that the terms $u_1 \cdot f_g^\perp$ and $u_2 \cdot f_g^\perp$ must have the same sign. The graphical interpretation of this fact is that z must lie *outside* the vertical strip S_2. Thus, x lies in the intersection $S_1^{+-} \cap \bar{S}_2$. By applying similar Considerations for the remaining two options $z \in \mathcal{C}_1^- \cap \mathcal{C}_2^-$ and $z \in \mathcal{C}_1^- \cap \mathcal{C}_2$, the final characterization of $\mathcal{R}(\boldsymbol{w}_o)$ is

$$\mathcal{R}(\boldsymbol{w}_o) = ((S_1^{++} \cup S_1^{--}) \cap S_2) \cup ((S_1^{+-} \cup S_1^{-+}) \cap \bar{S}_2).$$

□

Note that even though $\bar{S}_2$ is a non-connected region and $\mathcal{R}(\boldsymbol{w}_o)$ is a union of regions, it is always *a single connected strip*, as proven in Theorem 1.The graphic characterization of $\mathcal{R}(\boldsymbol{w}_o)$ is consistent with the characterization given in [6], in the context of object manipulation. It is also consistent with the analysis in [3] in the context of locomotion planning under gravity. Nevertheless, non of these works has explicitly formulated $\mathcal{R}(\boldsymbol{w})$ for an arbitrary number of contacts. Furthermore, non of these works has considered a general external wrench and a neighborhood of wrenches, as we do in this work.

Extension to a General External Wrench. We now generalize the graphic characterization of $\mathcal{R}(\boldsymbol{w})$ to a general wrench $\boldsymbol{w} = (f_{ext}, \tau_{ext})$. When $\tau_{ext} = 0$, the force f_{ext} acts at x but is rotated about the vertical direction of f_g. Therefore the feasible equilibrium region is constructed by the same procedure described above, except that now the vertical strips S_1 and S_2 are rotated as to match the direction of f_{ext}. When $\tau_{ext} \neq 0$, the wrench $\boldsymbol{w}$ is equivalent to a force f_{ext} which acts with a perpendicular offset d from x, where $d = \tau_{ext}/\|f_{ext}\|$. Hence the strips S_1 and S_2 are rotated and parallel shifted by $-d$ as shown in Figure 2(d).
The graphical characterization of $\mathcal{R}(\boldsymbol{w})$ for two contacts is extremely powerful, since according to proposition 2.1, it enables us to construct the k-contacts feasible equilibrium region as the convex hull of the regions associated with all pairs of contacts. A straightforward

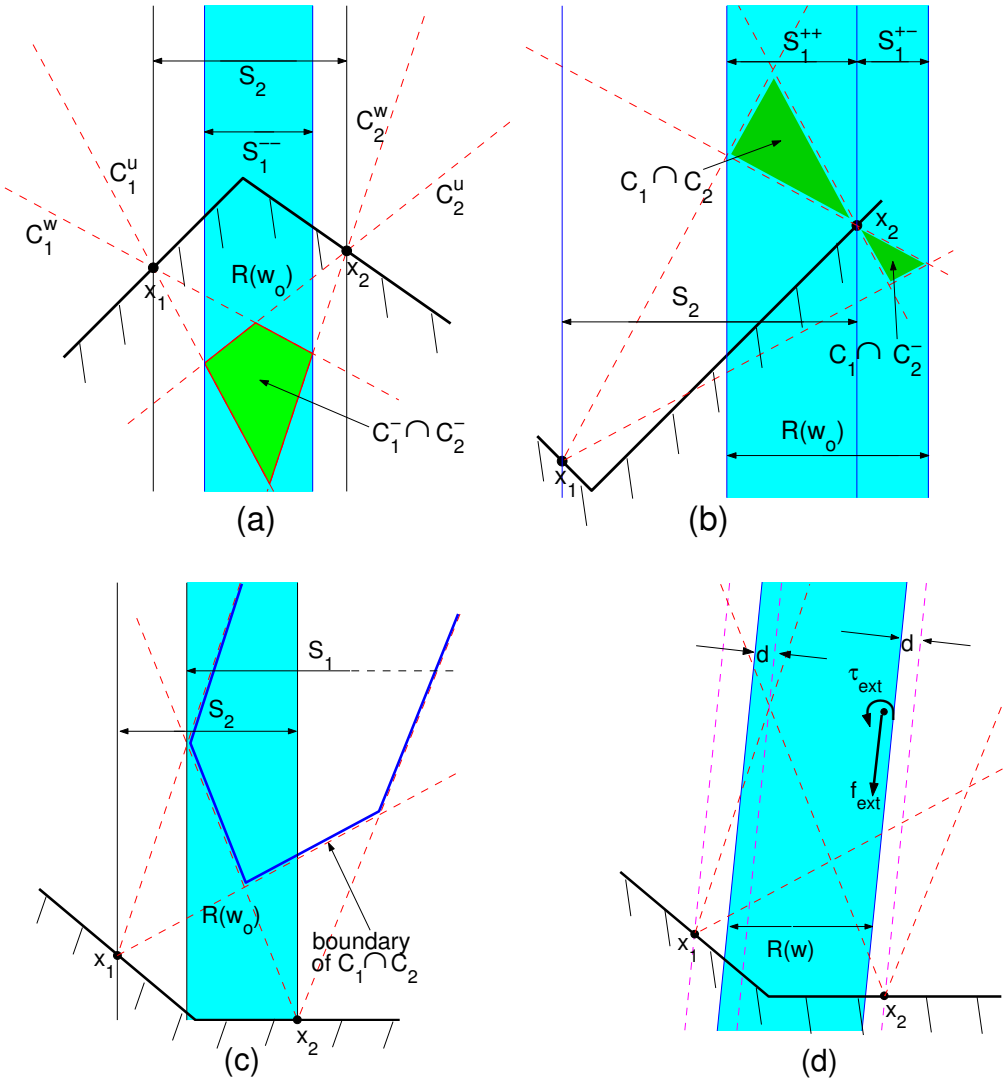

Figure 2: Graphic characterization of $\mathcal{R}(\boldsymbol{w})$ in four cases: (a)$\mathcal{R}(\boldsymbol{w}_o) = S_1^{--} \cap S_2$ (b)$\mathcal{R}(\boldsymbol{w}_o) = S_1^{++} \cup S_1^{+-}$ (c)$\mathcal{R}(\boldsymbol{w}_o) = S_1^{++} \cap S_2$ (d)$\mathcal{R}(\boldsymbol{w})$ for a general wrench $\boldsymbol{w} = (f_{ext}, \tau_{ext})$

computation requires inspection of all possible pairs of contacts, and hence requires $O(k^2)$ steps. In Appendix A we present a geometric algorithm for computing $\mathcal{R}(\boldsymbol{w})$ for k-contact postures, which is practically *linear* in k.

3 The Robust Equilibrium Region

So far we described the feasible equilibrium region for a particular external wrench $\boldsymbol{w}$ which is usually the nominal gravitational wrench. However, in practice one wishes to select *robust* postures that resist *a set* of external wrenches. Such sets originate mainly from inertial forces generated by moving internal limbs of the mechanism during quasistatic locomotion. But they can also originate from environmental causes such as vibrations or positioning inaccuracies. In this section we consider the computation of the *robust equilibrium region,* defined as $\mathcal{R}(\mathcal{W}) = \cap_{\boldsymbol{w}\in\mathcal{W}}\mathcal{R}(\boldsymbol{w})$, where $\mathcal{W}$ is a given neighborhood of disturbance wrenches centered at the nominal gravitational wrench. Any posture with $x \in \mathcal{R}(\mathcal{W})$ is robust in the sense that it generates a feasible equilibrium for *all* $\boldsymbol{w} \in \mathcal{W}$. First we describe a convenient parameterization for $\mathcal{W}$. Then we formulate the robust equilibrium region associated with $\mathcal{W}$ as an intersection of strips associated with the vertices of $\mathcal{W}$. Finally, we show some examples and a graphical characterization of $\mathcal{R}(\mathcal{W})$.

3.1 Parametrization of the Wrench Neighborhood $\mathcal{W}$

A key fact in the equilibrium condition (1) is that if the contact forces $\vec{f}$ satisfy (1) with an external wrench $\boldsymbol{w}$, then the contact forces $\alpha\vec{f}$ satisfy (1) with the external wrench $\alpha\boldsymbol{w}$ for any $\alpha > 0$. Hence feasibility of a static equilibrium posture does not depend on the particular magnitude of the external wrench. We exploit this fact in order to choose a convenient wrench parametrization. Let (f_x, f_y) denote the horizontal and vertical coordinates of f_{ext}. Since $f_{ext} = f_g + f_d$ such that f_g is vertical and $\|f_d\| \ll \|f_g\|$, we may assume that $f_y \neq 0$. Thus we define *homogeneous coordinates* for wrench space as (p, q), where $p \triangleq f_x/f_y$ and $q \triangleq \tau_{ext}/f_y$. The (p, q) coordinates can be interpreted as follows. The nominal gravitational wrench, $\boldsymbol{w}_o = (f_g, 0)$, corresponds to $(p, q) = (0, 0)$. Any other wrench $\boldsymbol{w} = (f_{ext}, \tau_{ext}) \in I\!R^2 \times I\!R$ can be represented by its magnitude and an oriented line of action. The wrench's line of action is oriented along f_{ext}, and the horizontal distance of the line from $\mathcal{B}$'s center-of-mass is τ_{ext}/f_y. Hence p represents the orientation of the wrench's line of action, and q represents its horizontal distance from x. Using (p, q), we assume that $\mathcal{W}$ is a *rectangular neighborhood* given by $\mathcal{W} = \{(p, q) : \kappa_1 \leq p \leq \kappa_2, \nu_1 \leq q \leq \nu_2\}$, where κ_i and ν_i are given parameters. Note that p represents orientation with respect to the fixed vertical direction, while q represents torques with resect to $\mathcal{B}$'s center-of-mass. The (p, q) parametrization is therefore independent of the particular choice of the world and body reference frames.

3.2 Computation of the Robust Equilibrium Region

We now compute the robust equilibrium region $\mathcal{R}(\mathcal{W})$. Using the (p, q) parametrization for the external wrenches, the equilibrium condition (2) becomes

$$\begin{bmatrix} G_f \\ G_\tau \end{bmatrix} \vec{f} = -\begin{pmatrix} p \\ 1 \\ \tau(x) \end{pmatrix} \quad \text{where } \vec{f} \geq \vec{0} \text{ and } \tau(x) = x^T J^T \begin{pmatrix} p \\ 1 \end{pmatrix} + q \,. \tag{5}$$

The following theorem characterizes the robust equilibrium region of $\mathcal{W}$.

Theorem 2. *Let $\mathcal{B}$ be supported by k frictional contacts in a two-dimensional gravitational field, and be subjected to a neighborhood $\mathcal{W} = [\kappa_1, \kappa_2]\times[\nu_1, \nu_2]$ of disturbance wrenches. Then the robust equilibrium region of $\mathcal{W}$ is the finite parallelogram given by*

$$\mathcal{R}(\mathcal{W}) = \big\{x : \tau_{i,min} - \nu_1 \le x^T J f^i_{ext} \le \tau_{i,max} - \nu_2 \text{ for } i = 1, 2\big\}, \tag{6}$$

where $f^i_{ext} = [\kappa_i \ 1]^T$, and $\tau_{i,min}, \tau_{i,max}$ are obtained by solving the linear programming problems:

$$\tau_{i,min} = \min_{G_f\vec{f}=-f^i_{ext}\,,\,\vec{f}\ge\vec{0}} \{-G_\tau\vec{f}\} \qquad \tau_{i,max} = \max_{G_f\vec{f}=-f^i_{ext}\,,\,\vec{f}\ge\vec{0}} \{-G_\tau\vec{f}\} \ \text{, for } i = 1, 2. \tag{7}$$

The graphic interpretation of (6) is a parallelogram obtained by intersection of the strips $\mathcal{R}(\boldsymbol{w}_{ij})$, where $\boldsymbol{w}_{ij}$ are the external wrenches parametrized by $(p, q) = (\kappa_i, \nu_j)$ for $1 \le i, j \le 2$.

Proof: First, we compute the region $\mathcal{R}$ defined as $\mathcal{R} = \mathcal{R}(\boldsymbol{w}_{11}) \cap \mathcal{R}(\boldsymbol{w}_{12}) \cap \mathcal{R}(\boldsymbol{w}_{21}) \cap \mathcal{R}(\boldsymbol{w}_{22})$. By definition, the wrench $\boldsymbol{w}_{ij}$ corresponds to the pair $(f_{ext}\,, \tau_{ext}\,)=(f^i_{ext}, \nu_j)$. Using Theorem 1 and the definition of $\tau_{i,min}, \tau_{i,max}$, the region $\mathcal{R}(\boldsymbol{w}_{ij})$ is the strip given by

$$\mathcal{R}(\boldsymbol{w}_{ij}) = \big\{x : \tau_{i,min} - \nu_j \le x^T J f^i_{ext} \le \tau_{i,max} - \nu_j\big\}.$$

Since ν_j appears as a linear additive term in $\mathcal{R}(\boldsymbol{w}_{ij}$, and $\nu_1 \le \nu_2$, the intersection region $\mathcal{R}$ can be written as

$$\mathcal{R} = \big\{x : \tau_{i,min} - \nu_1 \le x^T J f^i_{ext} \le \tau_{i,max} - \nu_2 \text{ for } i = 1, 2\big\}.$$

We now prove that $\mathcal{R}(\mathcal{W}) = \mathcal{R}$ in two steps. First we show that $\mathcal{R}(\mathcal{W}) \subseteq \mathcal{R}$, then we show that $\mathcal{R} \subseteq \mathcal{R}(\mathcal{W})$.

1. If $x \in \mathcal{R}(\mathcal{W})$, then by definition $x \in \mathcal{R}(\boldsymbol{w})$ for all $\boldsymbol{w} \in \mathcal{W}$. In particular, x lies in $\mathcal{R}(\boldsymbol{w}_{ij})$ for $i, j \in \{1, 2\}$. Recalling the definition of $\mathcal{R}$, we conclude that $x \in \mathcal{R}$.

2. If $x \in \mathcal{R}$, then by definition $x \in \mathcal{R}(\boldsymbol{w}_{ij})$ for $1 \le i, j \le 2$. Hence for any $i, j \in \{1, 2\}$ there exists a $2k$-vector $\vec{f}_{ij} \ge \vec{0}$ that satisfies the equilibrium condition

$$\begin{aligned} G_f\vec{f}_{ij} &= -f^i_{ext} \\ G_\tau\vec{f}_{ij} &= -(x^T J^T f^i_{ext} + \nu_j). \end{aligned} \tag{8}$$

   We now show that $x \in \mathcal{R}(\boldsymbol{w})$ for all $\boldsymbol{w} \in \mathcal{W}$. Any $\boldsymbol{w} \in \mathcal{W}$ can be parametrized by (p, q) within the rectangle $[\kappa_1, \kappa_2]\times[\nu_1, \nu_2]$, and hence can be represented as a convex combination of the vertices of $\mathcal{W}$. Therefore, we can assume that $\boldsymbol{w}$ is parametrized by $\binom{p}{q} = \sum_{i,j} \lambda_{ij}\binom{\kappa_i}{\nu_j}$ for some $\lambda_{ij} \in [0, 1]$ such that $\sum_{i,j} \lambda_{ij} = 1$ and $i, j \in \{1, 2\}$. Thus $\boldsymbol{w}$ corresponds to the pair $(f_{ext}\,, \tau_{ext}\,)=(f^\lambda_{ext}, \nu_\lambda)$, where $(f^\lambda_{ext} = (\lambda_{11} + \lambda_{12})f^1_{ext} + (\lambda_{21} + \lambda_{22})f^2_{ext}$ and $\nu_\lambda = (\lambda_{11} + \lambda_{21})\nu_1 + (\lambda_{21} + \lambda_{22})\nu_2$. We now wish to find a contact forces' vector $\vec{f} \in I\!R^{2k}$ that satisfies the equilibrium condition (5) with external wrench $\boldsymbol{w}$. Recall the definition of the $2k$-vectors $\vec{f}_{ij}$ satisfying (8). If one chooses a vector of contact forces $\vec{f}_\lambda = \sum_{i,j} \lambda_{ij}\vec{f}_{ij} \ge \vec{0}$, one gets

$$\begin{aligned} G_f\vec{f}_\lambda &= \textstyle\sum_{i,j} \lambda_{ij} G_f\vec{f}_{ij} = -(\lambda_{11} + \lambda_{12})f^1_{ext} - (\lambda_{21} + \lambda_{22})f^2_{ext} = -f^\lambda_{ext} \\ G_\tau\vec{f}_\lambda &= \textstyle\sum_{i,j} \lambda_{ij} G_\tau\vec{f}_{ij} = -x^T J^T((\lambda_{11} + \lambda_{12})f^1_{ext} + (\lambda_{21} + \lambda_{22})f^2_{ext}) \\ &\quad -((\lambda_{11} + \lambda_{21})\nu_1 + (\lambda_{21} + \lambda_{22})\nu_2) = -(x^T J^T f^\lambda_{ext} + \nu_\lambda) \end{aligned}$$

Thus $\vec{f}_\lambda$ satisfies the equilibrium condition (5) with $\boldsymbol{w} = (\vec{f}_\lambda, \nu_\lambda)$ and center-of-mass at x, and hence $x \in \mathcal{R}(\boldsymbol{w})$. Since this holds for *all* $\boldsymbol{w} \in \mathcal{W}$, we finally conclude that $x \in \mathcal{R}(\mathcal{W})$ $\square$

Notice that this Theorem can be easily extended to the case where the wrench neighborhood $\mathcal{W}$ is a general convex polygon in (p, q)-plane. In such case, $\mathcal{R}(\mathcal{W})$ is simply the intersection of the feasible equilibrium strips associated with the external wrenches corresponding to the vertices of $\mathcal{W}$.

We now show two examples of the construction of $\mathcal{R}(\mathcal{W})$.

Example 3: In the example shown in Figure 3(a), two frictional contacts are supporting $\mathcal{B}$ with $\mu = 0.4$. We have chosen a rectangular wrench neighborhood $\mathcal{W} = [-\kappa, \kappa] \times [0, \nu]$ with $\kappa = 0.3$ and $\nu = \|x_2 - x_1\|/8$. The figure shows the strips $\mathcal{R}(\boldsymbol{w}_{ij})$ associated with the vertices of $\mathcal{W}$. These strips can be computed using Theorem 1. Alternatively, they can be constructed using the graphic characterization for two-contact postures. The shaded region $\mathcal{R}(\mathcal{W})$ is the parallelogram obtained by the intersection of these four strips.

Example 4: In the example shown of in Figure 3(b), four contacts are supporting $\mathcal{B}$ with $\mu = 0.4.$, We have chosen a rectangular wrench neighborhood $\mathcal{W} = [-\kappa, \kappa] \times [-\nu, \nu]$ with $\kappa = 0.3$ and $\nu = \|x_4 - x_1\|/3$. In such case where $\nu_1 = -\nu_2$, the procedure for constructing $\mathcal{R}(\mathcal{W})$ is even more simple. One only needs to consider the two strips associated with the external wrenches $(f_{ext}\,, \tau_{ext}\,) = (f^i_{ext}, 0)$ for $i = 1, 2$. Then $\mathcal{R}(\mathcal{W})$ is obtained by taking the parallelogram obtained by the intersection of these two strips, and then shifting its edges *inward* by a horizontal distance of ν. The two strips and the resulting parallelogram $\mathcal{R}(\mathcal{W})$ are shown in Figure 3(b). Note that increasing the torque bound ν causes a shrinking of $\mathcal{R}(\mathcal{W})$, which may eventually become empty.

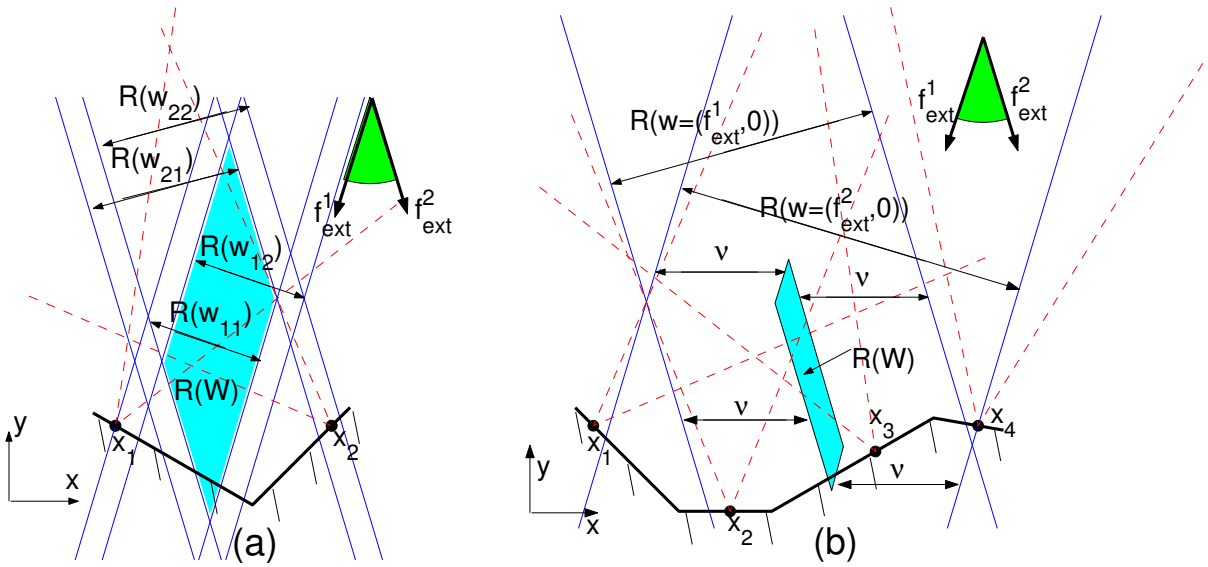

Figure 3: The region $\mathcal{R}(\mathcal{W})$ for (a)two and (b)four contacts

4 Generalization to Contact Patches

Finally, we generalize the results to cases where the contact is distributed on a region or a patch, rather than at a single point. Examples for such a contact are an edge-to-edge contact situation, and multi-limbed mechanisms with flat footpads (Figure 4(a)) on a piecewise linear terrain. A distributed contact generates normal and tangential traction fields $\sigma_n(r), \sigma_t(r)$, where r parametrizes points on the contact patch. As customary in the solid mechanics literature [9], we assume that the Coulomb friction law holds at every point of the contact patch, and states that $|\sigma_t(r)| \leq \mu\sigma_n(r)$, $\sigma_n(r) \geq 0$. The net force and moment generated by the contact patch is computed by integration as follows.

$$f = \int \sigma_n(r)n(r) + \sigma_t(r)t(r)dr \quad , \quad \tau = \int r \times \big(\sigma_n(r)n(r) + \sigma_t(r)t(r)\big)dr$$

In the planar case, the contact patch is a one-dimensional curve. Since we assume a piecewise linear terrain, the i-th patch is a line segment which can be parametrized as $r(s) = x_i^o + s_i t_i$, $s_i \in [0, L_i]$, where x_i^o is the i'-th patch's start point, L_i is the patch's length, and t_i is the unit tangent vector at the i-th contact patch. Let f_i^n and f_i^t be the net normal and tangential forces at the i'-th contact. Since n_i and t_i are constant along the patch, the local Coulomb friction law holds also for the net forces $|f_i^t| \leq \mu f_i^n$, $f_i^n \geq 0$. The net torque generated by the i-th contact is $x_i^o \cdot J^T f_i + \tau_i$, where $f_i = f_i^t t_i + f_i^n n_i$ and $0 \leq \tau_i \leq L_i f_i^n$. Therefore, the contact patch can be represented by a point contact at x_i^o, together with an additional torque τ_i whose bounds depend on the patch length L_i and the normal component f_i^n. Notice that a point contact can be represented as a zero length patch.
We can now compute the robust equilibrium region $\mathcal{R}(\mathcal{W})$ for contact patches using the same linear programming technique, with the additional parameters τ_i, as summarized in the following lemma.

Theorem 3. *Let $\mathcal{B}$ be supported by k frictional contact patches characterized by x_i^o, L_i, in a two dimensional gravitational field, and be subjected to a neighborhood $\mathcal{W} = [\kappa_1, \kappa_2] \times [\nu_1, \nu_2]$ of disturbance wrenches. Then the robust equilibrium region of $\mathcal{W}$ is the parallelogram given by*

$$\mathcal{R}(\mathcal{W}) = \big\{x : \tau_{i,min} - \nu_1 \leq x^T J f_{ext}^i \leq \tau_{i,max} - \nu_2 \text{ for } i = 1, 2\big\}, \tag{9}$$

where $f_{ext}^i = \begin{pmatrix} \kappa_i \\ 1 \end{pmatrix}$ and $\tau_{i,min}, \tau_{i,max}$ are obtained by solving the linear programming problems:

$$\tau_{i,min} = \min_{\widetilde{G}_f v = -f_{ext}^i \,,\, Av \geq 0 \,,\, v \geq 0} \{-\widetilde{G}_\tau v\} \qquad \tau_{i,min} = \min_{\widetilde{G}_f v = -f_{ext}^i \,,\, Av \geq 0 \,,\, v \geq 0} \{-\widetilde{G}_\tau v\} \quad , \text{ for } i = 1, 2. \tag{10}$$

$$\text{where } v \in I\!R^{3k} \quad , \quad \widetilde{G}_f = [G_f \quad 0_{2\times k}] \quad , \quad \widetilde{G}_\tau = [G_\tau \; 1 \cdots 1]_{1\times 3k}$$

$$A = \begin{bmatrix} [\mathsf{diag}(b_i)]_{k\times 2k} & -I_{k\times k} \end{bmatrix} \quad , \quad b_i = L_i \cos(\gamma) \cdot [1 \;\; 1] \quad , \quad \gamma = \tan^{-1}(\mu)$$

Proof: The contact response parameters now consist of the contact forces $\vec{f}$ acting at the nominal points x_j^o, and the additional patch torques $\vec{\tau} = [\tau_1 \cdots \tau_k]^T$. Let us now define the vector of combined parameters $v = (\vec{f}, \vec{\tau})$. The force balance is $G_f \vec{f} = -f_{ext}$ as stated in Eq. (2). The torque balance now becomes $x_1^T J^T f_1 + \tau_1 + \cdots + x_k^T J^T f_k + \tau_k = -\tau_o$. Using the

augmented matrices $\widetilde{G}_f, \widetilde{G}_\tau$ defined above, the equilibrium equations can now be rewritten in terms of v as follows.

$$\begin{pmatrix} \widetilde{G}_f \\ \widetilde{G}_\tau \end{pmatrix} v = - \begin{pmatrix} f_{ext} \\ \tau(x) \end{pmatrix} \quad \text{where } \tau(x) = x^T J^T f_{ext} + \tau_{ext} \tag{11}$$

In order to complete the formulation of equilibrium conditions, we now have to add the inequality constraints. Since $\vec{f}$ and $\vec{\tau}$ need to be nonnegative, we can write $v \geq 0$. Finally, we have to write the patch torque constraints $\tau_j \leq L_j f_j^n$. Since $\vec{f}$ is defined in terms of f_j^u, f_j^w, we use the transformation

$$\begin{pmatrix} f_j^t \\ f_j^n \end{pmatrix} = \begin{bmatrix} sin(\gamma) & -sin(\gamma) \\ cos(\gamma) & cos(\gamma) \end{bmatrix} \begin{pmatrix} f_j^u \\ f_w^j \end{pmatrix} \text{ to write } \tau_j \leq L_j cos(\gamma) \begin{bmatrix} 1 & 1 \end{bmatrix} \begin{pmatrix} f_j^u \\ f_w^j \end{pmatrix}$$

Using the augmented matrix A defined above, these inequalities can now be written in matrix form as $Av \geq 0$. After formulating the static equilibrium conditions and constraints for frictional contact patches, the interpretation of $\tau_{i,min}$ and $\tau_{i,max}$ is just the same as in the proof of Theorem 2, and the same considerations are followed for constructing $\mathcal{R}(\mathcal{W})$. □

In the example shown in Figure 4(a), a biped mechanism is standing with flat footpads that generate contact patches with the terrain. Each contact patch is characterized by its start point x_i^o, its length L_i, and its tangent vector t_i. The patch's endpoint is denoted x_i^L, where $x_i^L = x_i^0 + L_i t_i$. Figure 4(b) shows the feasible equilibrium region $\mathcal{R}(\boldsymbol{w}_o)$ for the nominal gravitational wrench $\boldsymbol{w}_o$. One can easily be convinced that $\mathcal{R}(\boldsymbol{w}_o)$ can be equivalently computed by considering the case of the four point contacts at $x_1^o, x_1^L, x_2^o, x_2^L$. This is because point contacts at the patch's ends x_i^o, x_i^L can generate exactly the same combination of contact forces and torques as the contact patch itself. Figure 4(c) shows the robust equilibrium region $\mathcal{R}(\mathcal{W})$ associated with the disturbance neighborhood $\mathcal{W} = [-\kappa, \kappa] \times [-\nu, \nu]$, where $\kappa = 0.3$ and $\nu = \|x_1^o - x_2^L\|/20$.

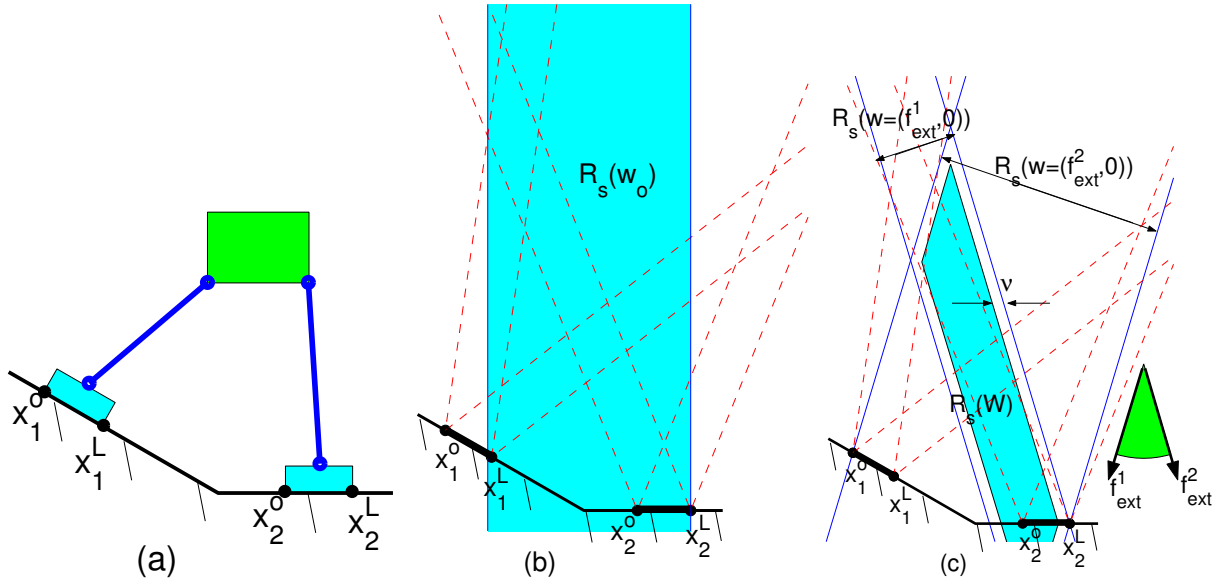

Figure 4: contact patch example -
(a)A biped mechanism with flat footpads. (b)The region $\mathcal{R}(\boldsymbol{w}_o)$ (c)The region $\mathcal{R}(\mathcal{W})$

5 Experimental Results

In this section we present results of preliminary experiments. The that test the static equilibrium of a mechanism in frictional contact with a variable terrain, under disturbance forces. The goal of this experiment is to validate the static analysis of feasible equilibrium conditions in frictional contact environment, under gravity and disturbance forces. Although the center-of-mass remains fixed in this experiment, the feasible equilibrium conditions in terms of disturbance forces can be obtained graphically in a way similar to the constructions in section 2, and are tested experimentally.

The experimental system consists of a two-limbed mechanism prototype made of Aluminium, whose center-of-mass position can be changed by mounting a heavy weight on an upper bar with adjustable angle. The mechanism is placed on a rigid V-shaped terrain of two segments with adjustable slopes. A horizontal force is applied on the mechanism by a variable weight hung on a string through a pulley. In our experiment, the mechanism was positioned on a symmetric V-shaped terrain with slope angles of $\alpha = 26.7^o$. The applied horizontal force is then gradually increased until reaching a critical value at which the contacts break or slip. The critical force was then recorded, and this process was repeated for different heights of the horizontal force's application point. The experiment setup is shown in figure 5. As a preliminary step, The coefficient of friction was experimentally measured by putting the mechanism on a single horizontal segment, and then gradually increasing its slope angle until sliding starts. The resulting critical slope angle is the angle of friction $\gamma = \tan^{-1}(\mu)$. Conducting these measurements resulted in critical angle of $\gamma = 13.8^o$ and hence $\mu = 0.25$ with a standard deviation of $\pm 6.5\%$.

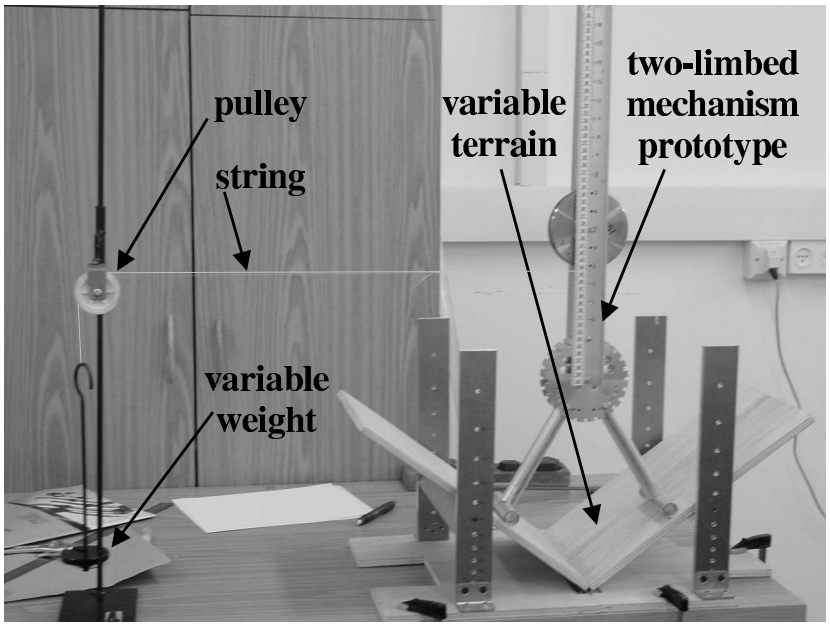

Figure 5: Experimental setup of equilibrium postures testing

In order to analyze the problem and predict the expected results, let us denote the horizontal distance between the contacts as l, and the height of the horizontal force application

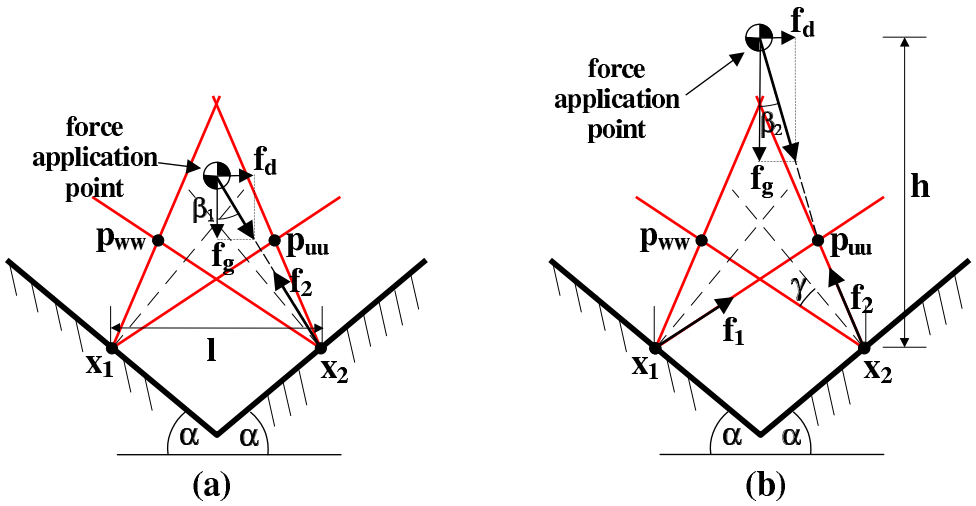

Figure 6: Graphic characterization of critical horizonal force for cases A and B

point about the contact points as h. Also, let f_g be the gravitational force, which is the mechanism's (constant) weight. The horizontal force f_d is variable, and the total applied force is rotated by the angle $\beta = \tan^{-1}(f_d/f_g)$ about the vertical direction. Although the static response of contact forces is indeterminate, the two possible critical cases of contact breakage or slippage are determinate, and can be obtained graphically as follows.

The first critical case occurs when the total applied force line intersects the contact point x_2, as shown in figure 6(a). At such case, the contact force on x_1 vanishes, resulting in contact breakage at x_1, and rolling about x_2. The corresponding critical force angle is $\beta_1 = tan^{-1}(l/2h)$. The second critical case occurs when the total applied force intersects the point p_{uu} , as shown in figure 6(b). At such a case the contact forces lie on the edges of their respective friction cones, and sliding starts at both contacts. From geometric relations, the corresponding critical force angle is $\beta_2 = tan^{-1}(sin2\gamma/(2hsin2\gamma/l - cos2\alpha - cos2\gamma))$. The critical force F_d for which the equilibrium conditions are violated, is the minimum value $F_{cr} = F_g tan(\beta_{cr})$, where $\beta_{cr} = \min\{\beta_1, \beta_2\}$. From graphical considerations, it is easy to distinguish between two possible cases. In the first case, the application point of F_g lies inside the polygon $\mathcal{C}_1 \cap \mathcal{C}_2$, as in Figure 6(a), and hence $\beta_1 < \beta_2$, and rolling will start. In the second case, the application point of F_g lies above the polygon $\mathcal{C}_1 \cap \mathcal{C}_2$, as in Figure 6(b), and hence $\beta_2 < \beta_2$, and sliding will start.

The experiments results are presented in Figure 7. For each force application height h, five experiments were conducted, the average critical force F_{cr} was measured, and its corresponding angle β_{cr} was computed. In order to present a linear relationship, we plot $cot(\beta_{cr})$ as a function of h. The dashed and solid lines are $cot(\beta_1)$ and $cot(\beta_2)$ respectively, calculated analytically as a function of h. Since $\beta_{cr} = \min\{\beta_1, \beta_2\}$, the experimental results were expected to follow the line of $cot(\beta_1)$ up to $h = 517$, then follow the line of $cot(\beta_2)$ for $h > 517$. The experimental results are marked as dots, with error bars of two standard deviations. One can see a close matching of the predicted behavior and the experimental results.

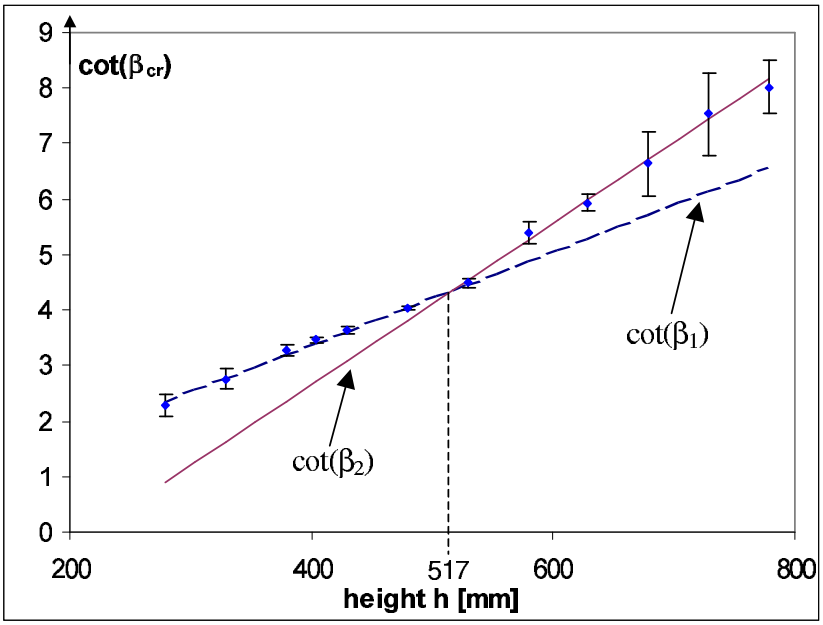

Figure 7: Experimental and theoretical results of $cot(\beta_{cr})$ as a function of h

6 3D Frictional Equilibrium Postures

In this section we generalize the results for three dimensional environments. First we present the conditions for a frictional equilibrium posture in 3D, and discuss some basic properties of the feasible equilibrium region. Then we focus on 3-contact postures and present a convenient parametrization of the static reaction forces for three contacts. Finally, we characterize he feasible equilibrium region using this parametrization and give a simple closed form approximation for its boundary.

6.1 Frictional Equilibrium in 3D

Given a solid object $\mathcal{B}$ supported by k frictional contacts under gravity, the equilibrium condition is given by

$$\sum_{i=1}^{k} \begin{pmatrix} I \\ [x_i\times] \end{pmatrix} \vec{f_i} = - \begin{pmatrix} I \\ \boldsymbol{x}\times \end{pmatrix} \vec{f_g} \tag{12}$$

where x_i is the position of the i^{th} contact, $\boldsymbol{x}$ is the position of $\mathcal{B}$'s center-of-mass, $\vec{f_i}$ is the i^{th} contact reaction force, f_g is the gravitational force acting at $\boldsymbol{x}$, and $[a\times]$ is the cross-matrix satisfying $[a\times]v = a \times v$ for all $v \in I\!R^3$. Additionally, the contact forces must lie in their respective friction cones

$$\mathcal{C}_i = \{\vec{f_i} : \vec{f_i} \cdot n_i \geq 0 \text{ and } (\vec{f_i} \cdot s_i)^2 + (\vec{f_i} \cdot t_i)^2 \leq (\mu \vec{f_i} \cdot n_i)^2\}, \tag{13}$$

where μ is the coefficient of friction, n_i is the outward unit normal at x_i, and s_i, t_i are unit tangents at x_i, such that (s_i, t_i, n_i) is a right-handed orthonormal frame. The friction

constraints can also be written as the following linear and quadratic inequalities;

$$\mathcal{C}_i = \{\vec{f_i} : \vec{f_i} \cdot n_i \geq 0 \text{ and } \vec{f_i}^T B_i \vec{f_i} \leq 0\} \text{ , where } B_i = [s_i \;\; t_i \;\; n_i] \cdot \mathsf{diag}(1, 1, -\mu^2) \cdot [s_i \;\; t_i \;\; n_i]^T. \tag{14}$$

In the following, we assume that all contacts are *upward pointing*, in the sense that all forces $\vec{f_i}$ in $\mathcal{C}_i$ satisfy $\vec{f_i} \cdot e \geq 0$. This is a reasonable assumption in the context of legged locomotion, since relevant supports are generally located *under* the robot's footpads. For a given set of contacts $x_1 \ldots x_k$, the 3D feasible equilibrium region ,denoted $\mathcal{R}_{3D}$, is all center-of-mass locations for which there exist contact reaction forces $\vec{f_i} \in \mathcal{C}_i$ that satisfy the static equilibrium condition (12). The following lemma summarizes some basic properties of $\mathcal{R}_{3D}$.

Lemma 6.1. *Given a solid body $\mathcal{B}$ supported by k frictional contacts under gravity, the feasible equilibrium region $\mathcal{R}_{3D}$, if nonempty, is an infinite vertical prism. This prism is a single connected set and its cross-section is convex. Furthermore, if $\mathcal{R}_{3D}$ is non-empty,its diension for k contacts is generically* $\min\{3, k\}$.

Proof: Let $\boldsymbol{e} = (0\ 0\ 1)$ denote the vertical direction. If $\boldsymbol{x} \in \mathcal{R}_{3D}$, then the infinite vertical line $\{\boldsymbol{x} + \beta \boldsymbol{e}, \beta \in I\!R\}$ is contained in $\mathcal{R}_{3D}$, since $\vec{f_g} \parallel \boldsymbol{e}$, and hence the right side of (12) is independent of β. Therefore $\mathcal{R}_{3D}$ is an infinite vertical prism.
next, let $\boldsymbol{x}'$ and $\boldsymbol{x}''$ be two points in $\mathcal{R}_{3D}$, and let $\vec{f_i'}, \vec{f_i''} \in \mathcal{C}_i$ be the corresponding contact forces for $i = 1 \ldots k$. Let $\boldsymbol{x}(\lambda) = \lambda \boldsymbol{x}' + (1 - \lambda)\boldsymbol{x}''$ for $\lambda \in [0, 1]$. It is easy to see that the contact forces $\vec{f_i} = \lambda \vec{f_i'} + (1 - \lambda)\vec{f_i''}$ lie in $\mathcal{C}_i$ and satisfy (12) with $\boldsymbol{x} = \boldsymbol{x}(\lambda)$. Therefore $\mathcal{R}_{3D}$ is connected as well as convex.
Finally, let us examine the dimension of $\mathcal{R}_{3D}$. Consider the geometric implications of (12) in wrench space. On the right side of (12), $\boldsymbol{x}$ parametrizes a two-dimensional affine subspace L in wrench space. (Note that the component of $\boldsymbol{x}$ along $\boldsymbol{e}$ is mapped to zero). On the left side of (12), the contact forces $\vec{f_i} \in \mathcal{C}_i$ parametrize a cone N in wrench space. The intersection $N \cap L$ determines the horizontal components of all points $\boldsymbol{x}$ in $\mathcal{R}_{3D}$, which gives the horizontal cross-section of $\mathcal{R}_{3D}$. For a single contact, the cone N is 3-dimensional in wrench space. However, wrenches $(\vec{f}, \vec{\tau}) \in I\!R^6$ generated by a *single* force must satisfy the additional scalar constraint $\vec{f} \cdot \vec{\tau} = 0$. Therefore, if $N \cap L$ is nonempty, it is zero-dimensional[1], i.e. a single point in wrench space. Physically, $\mathcal{R}_{3D}$ is the infinite vertical line passing through the single contact. When $k = 2$ the wrench cone N is *five*-dimensional, since $\vec{f_1}$ and $\vec{f_2}$ cannot generate torques about the line connecting x_1 and x_2. Therefore $N \cap L$ is generically one-dimensional. In this case $\mathcal{R}_{3D}$ is an infinite vertical strip lying in the vertical plane passing through x_1 and x_2. When $k \geq 3$, N is a six-dimensional cone in wrench space, and $N \cap L$ is generically a two-dimensional region in wrench space. Each point in $N \cap L$ determines an infinite vertical line in $\mathcal{R}_{3D}$, which is consequently three-dimensional. □
The analysis of the dimension of $\mathcal{R}_{3D}$ was first presented in [15] for frictionless contact postures in 3D, and was extended here for the frictional case.
The problem of computing the prism $\mathcal{R}_{3D}$ is thus reduced to computing its horizontal cross-section, denoted $\widetilde{\mathcal{R}}_{3D}$, in $I\!R^2$. Since $k = 3$ is the smallest number of contacts for which $\mathcal{R}_{3D}$ is fully three-dimensional, the remainder of this section focuses on the computation of $\widetilde{\mathcal{R}}_{3D}$ for 3-contact postures.

[1] In general, if M is an m-dimensional manifold and N is an n-dimensional manifold in $I\!R^p$, the intersection $M \cap N$, if nonempty, has dimension $m + n - p$.

The Support Polygon Principle: The classical *support polygon principle* appears in the legged locomotion literature [16], as a measure for frictionless postures' static stability on flat horizontal surfaces. This principle (also known as *the tripod rule* in 3-legged cases) states that the center-of-mass must lie in a vertical prism whose horizontal cross section is the *support polygon* — the convex hull of the horizontal projections of all contact points. This principle is easily extended to the frictional case as long as the supports are *nearly flat*, i.e. the upward direction $\boldsymbol{e}$ is contained in *all* friction cones $\mathcal{C}_i$. In such cases, the support polygon serves as a practical conservative approximation for $\widetilde{\mathcal{R}}_{3D}$. However, in non-flat cases where some of the friction cones *do not* contain $\boldsymbol{e}$, this principle cannot be applied. The method presented in this section applies also for non-flat cases, as long as all contacts are *upward pointing*.

6.2 Static Forces in 3-Contact Postures

We now focus on 3-contact postures and present a parametrization for the static reaction forces satisfying (12) and (14). The resulting parametrization would be in terms of a parameter $\boldsymbol{r}$ which varies within a polygonal region in $I\!R^2$, and $\boldsymbol{\zeta}$ which varies in $I\!R^3$. Let us decompose each contact force into its horizontal and vertical projections,

$$\tilde{f}_i = E^T \vec{f}_i \ \ , \ \ f_i^z = \boldsymbol{e} \cdot \vec{f}_i \ , \text{ where } E = \begin{pmatrix} 1 & 0 \\ 0 & 1 \\ 0 & 0 \end{pmatrix}.$$

Let $\tilde{\boldsymbol{x}} = E^T \boldsymbol{x}$ be the horizontal projection of $\boldsymbol{x}$. Then the equilibrium condition can be divided into three equation sets [15]

$$\begin{aligned} &a. \quad \textstyle\sum_{i=1}^3 \tilde{f}_i = 0_{2\times 1} \\ &\qquad \boldsymbol{e}^T \textstyle\sum_{i=1}^3 [x_i\times]\, E\tilde{f}_i = 0 \\ &b. \quad \textstyle\sum_{i=1}^3 f_i^z = 1 \\ &c. \quad \textstyle\sum_{i=1}^3 H_i\tilde{f}_i + h_i f_i^z = J^T\tilde{\boldsymbol{x}}, \end{aligned} \tag{15}$$

where $H_i = E^T[x_i\times]E$, $h_i = E^T[x_i\times]\boldsymbol{e}$, and $J = \left[\begin{smallmatrix} 0 & -1 \\ 1 & 0 \end{smallmatrix}\right]$. Note that the force units are scaled such that $\|\vec{f}_g\| = 1$. We will use (15a) and (15b) to obtain a parametrization of the contact forces, which will then imply a parametrization for $\boldsymbol{x}$ via Eq. (15c). The three scalar equations (15a) are force and torque balance of the three contact forces in a horizontal plane. These equations are independent of $\boldsymbol{x}$, contain six scalar unknowns, and hence are indeterminate of degree 3. Let $\tilde{x}_i = E^T x_i$ be the horizontal projection of the contact point x_i, and let $\tilde{\mathcal{C}}_i$ be the horizontal projection of the friction cone $\mathcal{C}_i$. In order to satisfy the friction constraints, $\tilde{f}_i$ must lie in $\tilde{\mathcal{C}}_i$. Since the horizontal forces $\tilde{f}_i$ generate zero net force and torque in the plane, they must intersect at a common point $\boldsymbol{r}$ in the plane. Since (15a) is homogenous in $\tilde{f}_i$, any particular choice of $\boldsymbol{r}$ determines $\tilde{f}_i$ up to a scaling factor $\sigma \in I\!R$. Therefore the pair $(\boldsymbol{r}, \sigma)$ fully parametrize $\tilde{f}_i$. Moreover, the frictional constraints imply that $\boldsymbol{r}$ must lie within a polygonal region in $I\!R^2$. These results are summarized in the following lemma.

Lemma 6.2. *Let $\boldsymbol{r}$ be a point in $\mathbb{R}^2$, and let $\sigma \in \mathbb{R}$ be a scaling factor. Then the horizontal contact forces solving Eq. (15a) are parametrized by $(\boldsymbol{r}, \sigma)$ as follows:*

$$\tilde{f}_i = \sigma\lambda_i(\boldsymbol{r})(\boldsymbol{r} - \tilde{x}_i) \ , \text{ where } \lambda_i(\boldsymbol{r}) = (\boldsymbol{r} - \tilde{x}_{i+1}) \cdot J(\tilde{x}_{i+2} - \tilde{x}_{i+1}) \ \ i = 1, 2, 3, \tag{16}$$

where the index i is taken modulo 3.
Furthermore, for any nontrivial solution satisfying $\tilde{f}_i \in \tilde{\mathcal{C}}_i$, $\boldsymbol{r}$ must lie within a union of two polygons $P = P_+ \cup P_-$, defined by:

$$\begin{aligned} P_+ &= \{\boldsymbol{r} : \ \ \mathsf{sgn}[\lambda_i(\boldsymbol{r})] \cdot (\boldsymbol{r} - \tilde{x}_i) \in \tilde{\mathcal{C}}_i \ , \ \boldsymbol{r} \neq \tilde{x}_i \ , \text{ for } i = 1, 2, 3\}, \\ P_- &= \{\boldsymbol{r} : \ \ -\mathsf{sgn}[\lambda_i(\boldsymbol{r})] \cdot (\boldsymbol{r} - \tilde{x}_i) \in \tilde{\mathcal{C}}_i \ , \ \boldsymbol{r} \neq \tilde{x}_i \ , \text{ for } i = 1, 2, 3\}. \end{aligned} \tag{17}$$

Proof: Eq. (15a) describes an equilibrium of three planar forces $\tilde{f}_1, \tilde{f}_2, \tilde{f}_3$. Since the three forces generate zero net torque, their lines must intersect at $\boldsymbol{r}$. Hence each force $\tilde{f}_i$ is directed from $\tilde{x}_i$ to $\boldsymbol{r}$ and can be written as $\tilde{f}_i = \sigma_i(\boldsymbol{r} - \tilde{x}_i)$ for some $\sigma_i \in \mathbb{R}$. The force part of (15a) can now be written as

$$\sigma_1(\boldsymbol{r} - \tilde{x}_1) + \sigma_2(\boldsymbol{r} - \tilde{x}_2) + \sigma_3(\boldsymbol{r} - \tilde{x}_3) = 0_{2\times 1}.$$

Taking dot product with $J(\boldsymbol{r} - \tilde{x}_1)$ and $J(\boldsymbol{r} - \tilde{x}_2)$, gives

$$\begin{aligned} (\boldsymbol{r} - \tilde{x}_2) \cdot J(\boldsymbol{r} - \tilde{x}_1)\sigma_2 + (\boldsymbol{r} - \tilde{x}_3) \cdot J(\boldsymbol{r} - \tilde{x}_1)\sigma_3 = 0 \\ (\boldsymbol{r} - \tilde{x}_1) \cdot J(\boldsymbol{r} - \tilde{x}_2)\sigma_1 + (\boldsymbol{r} - \tilde{x}_3) \cdot J(\boldsymbol{r} - \tilde{x}_2)\sigma_3 = 0 \end{aligned}$$

This is a homogenous linear system in $\sigma_1, \sigma_2, \sigma_3$. Its solution up to a scaling factor $\sigma \in \mathbb{R}$ is

$$\sigma_i = \sigma(\boldsymbol{r} - \tilde{x}_{i+2}) \cdot J(\boldsymbol{r} - \tilde{x}_{i+1}), \text{ where the index } i \text{ is taken modulo 3.}$$

Substituting the identity $(\boldsymbol{r} - \tilde{x}_{i+2}) \cdot J(\boldsymbol{r} - \tilde{x}_{i+1}) = (\boldsymbol{r} - \tilde{x}_{i+1}) \cdot J(\tilde{x}_{i+2} - \tilde{x}_{i+1}) = \lambda_i(\boldsymbol{r})$, we obtain the solution (16). Finally, each force $\tilde{f}_i = \sigma\lambda_i(\boldsymbol{r}) \cdot (\boldsymbol{r} - \tilde{x}_i)$ must lie in its friction cone $\tilde{\mathcal{C}}_i$. Due to the homogeneity of the cone $\tilde{\mathcal{C}}_i$ in $\tilde{f}_i$, only the *sign* of $\sigma\lambda_i(\boldsymbol{r})$ matters. Note that $\sigma = 0$, or $\boldsymbol{r} = \tilde{x}_i$ for some i, yield the trivial solution $\tilde{f}_1 = \tilde{f}_2 = \tilde{f}_3 = 0_{2\times 1}$. Hence σ can be either positive or negative, but not zero. Considering both cases for $\mathsf{sgn}(\sigma)$, the region $P_+ \cup P_-$ in (17) is obtained. □

Example: Figure 9 shows two 3-contact arrangements in 3D, together with the friction cones $\mathcal{C}_i$ for $\mu = 0.2$. Figure 10 shows the projections of the contacts $\tilde{x}_i$ onto the horizontal plane, together with the projected friction cones $\tilde{\mathcal{C}}_i$. In Figure 10a the shaded region $P = P_+$ is simply the intersection of the three cones $\tilde{\mathcal{C}}_i$. In Figure 10b the shaded region is $P = P_+ \cup P_-$, where $P_+ = \tilde{\mathcal{C}}_1 \cap \tilde{\mathcal{C}}_2 \cap \tilde{\mathcal{C}}_3$, and P_- is the intersection of $\tilde{\mathcal{C}}_1$ and $\tilde{\mathcal{C}}_2$ with the negative reflection of $\tilde{\mathcal{C}}_3$. In both contact arrangements, the horizontal forces $\tilde{f}_i$ are parametrized by $(\boldsymbol{r}, \sigma)$, such that $\boldsymbol{r} \in P$ and $\sigma \in \mathbb{R}$.
Our next step is to extend the parametrization of the horizontal forces to a parametrization of the full contact forces by the pair $(\boldsymbol{r}, \boldsymbol{\zeta}) \in \mathbb{R}^2 \times \mathbb{R}^3$, where the intermediate parameter σ is eliminated. Recall that $\boldsymbol{r}$ is the planar intersection point of $\tilde{f}_i$. Let l_r be the vertical line in $\mathbb{R}^3$ whose horizontal projection is $\boldsymbol{r}$. A natural choice for parametrizing the vertical component of $\vec{f}_i$ is ζ_i—the vertical distance between the contact x_i and the point where the line of $\vec{f}_i$ intersects the vertical line l_r (Figure 11a). Let $\boldsymbol{\zeta} = (\zeta_1, \zeta_2, \zeta_3)$. We now define Q

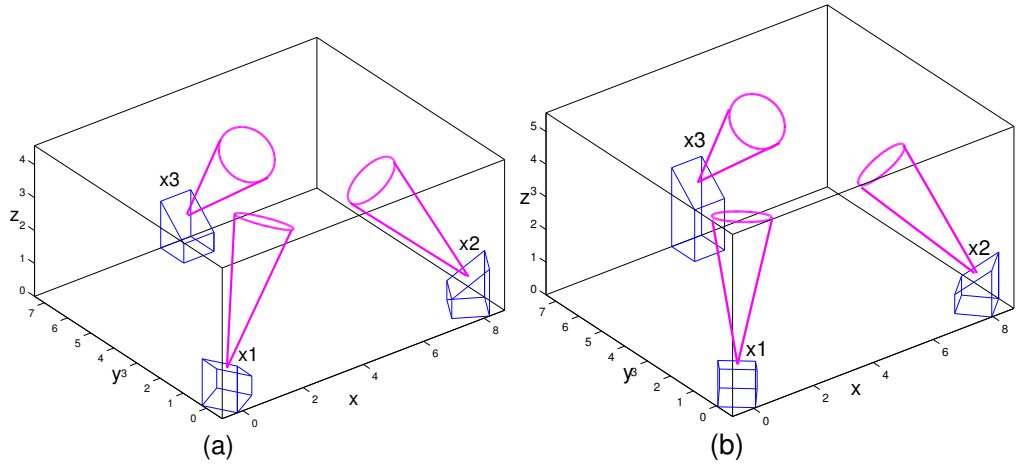

Figure 8: Two three-contact arrangements with $\mu = 0.2$.

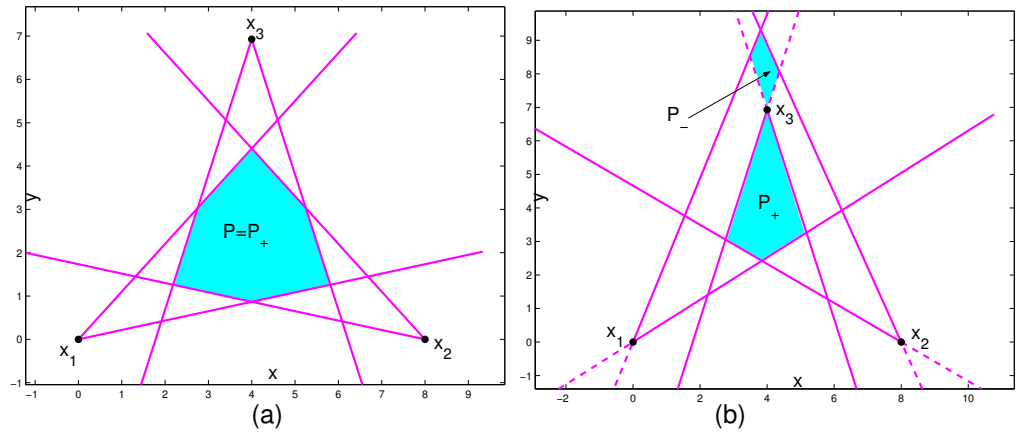

Figure 9: The horizontal projection of the contacts and friction cones, and the resulting region P (shaded).

as the permissible region of $(\boldsymbol{r}, \boldsymbol{\zeta})$ implied by the frictional constraints (13), and analyze its structure. The projection of Q onto the $\boldsymbol{r}$-plane is the polygonal region P defined in (17). Let Π be the vertical prism in $I\!R^3$ whose horizontal cross-section is P. The pair $(\boldsymbol{r}, \zeta_i)$ determine the direction of $\vec{f_i}$. Its permissible region, denoted $\tilde{Q}_i$, is obtained by the intersection of the prism Π and the friction cone $\mathcal{C}_i$ in the physical space (Figure 11b). Therefore, Q is the intersection $Q_1 \cap Q_2 \cap Q_3$, where Q_i is the cylinder obtained by properly lifting $\tilde{Q}_i$ to $(\boldsymbol{r}, \boldsymbol{\zeta})$ space. The following lemma summarizes the parametrization of the contact forces $\vec{f_i}$ by the pair $(\boldsymbol{r}, \boldsymbol{\zeta})$, and formulates the permissible region Q.

Lemma 6.3. *The full contact forces solving equations (15a) and (15b) are parametrized by* $(\boldsymbol{r}, \boldsymbol{\zeta}) \in I\!R^2 \times I\!R^3$ *as follows:*

$$\vec{f_i} = \sigma(\boldsymbol{r}, \boldsymbol{\zeta}) \lambda_i(\boldsymbol{r}) (E(\boldsymbol{r} - \tilde{x}_i) + \zeta_i \boldsymbol{e}) \text{ for } i = 1, 2, 3, \tag{18}$$

where $\lambda_i(\boldsymbol{r}) = (\boldsymbol{r} - \tilde{x}_{i+1}) \cdot J(\tilde{x}_{i+2} - \tilde{x}_{i+1})$, *and* $\sigma(\boldsymbol{r}, \boldsymbol{\zeta}) = 1/(\lambda_1(\boldsymbol{r})\zeta_1 + \lambda_2(\boldsymbol{r})\zeta_2 + \lambda_3(\boldsymbol{r})\zeta_3)$. *Furthermore, in order to satisfy* $\vec{f_i} \in \mathcal{C}_i$, *the parameters* $(\boldsymbol{r}, \boldsymbol{\zeta})$ *must lie within a region* Q *in* $I\!R^2 \times I\!R^3$, *defined by:*

$$\begin{aligned} Q = \{(\boldsymbol{r}, \boldsymbol{\zeta}) : \boldsymbol{r} \in P \ , \ \sigma(\boldsymbol{r}, \boldsymbol{\zeta}) \lambda_i(\boldsymbol{r}) \zeta_i \geq 0, \text{ and} \\ \sigma(\boldsymbol{r}, \boldsymbol{\zeta}) \lambda_i(\boldsymbol{r}) (E(\boldsymbol{r} - \tilde{x}_i) + \zeta_i \boldsymbol{e})^T B_i (E(\boldsymbol{r} - \tilde{x}_i) + \zeta_i \boldsymbol{e}) \leq 0 \text{ for } i = 1, 2, 3\}. \end{aligned} \tag{19}$$

Proof: As shown in Lemma 6.2, choosing $\tilde{f}_i = \sigma\lambda_i(\boldsymbol{r})(\boldsymbol{r} - \tilde{x}_i)$ satisfies Eq. (15a) for any value of σ. Choosing $f_z^i = \sigma\lambda_i(\boldsymbol{r})\zeta_i$ and substituting into (15b) gives $(\lambda_1(\boldsymbol{r})\zeta_1 + \lambda_2(\boldsymbol{r})\zeta_2 + \lambda_3(\boldsymbol{r})\zeta_3)\sigma = 1$. Therefore $\sigma = 1/(\lambda_1(\boldsymbol{r})\zeta_1 + \lambda_2(\boldsymbol{r})\zeta_2 + \lambda_3(\boldsymbol{r})\zeta_3)$ solves Eq. (15b). It was also shown in Lemma 6.2 that $\boldsymbol{r}$ must lie in P. Since we assumed *upward pointing* contacts, the linear inequalities $n_i \cdot \vec{f}_i \geq 0$ in (14) can be replaced with $f_i^z \geq 0$. Finally, substituting the expression (18) for $\vec{f}_i(\boldsymbol{r}, \boldsymbol{\zeta})$ into the quadratic friction cone constraint in (14) yields the second inequality in (19). □

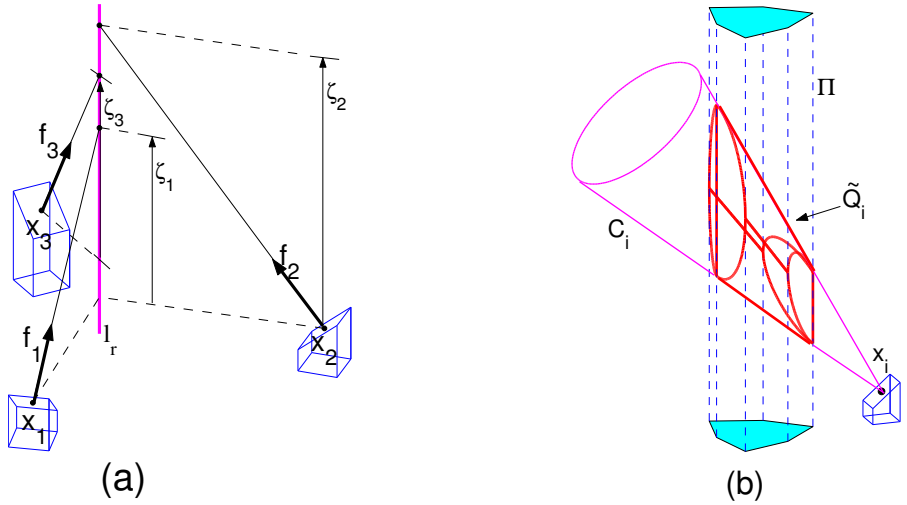

Figure 10: (a) Graphic illustration of ζ_i. (b) The permissible region $\tilde{Q}_i$ in physical space.

6.3 A Conservative Approximation for $\mathcal{R}_{3D}$

The three reaction forces are parametrized by the parameters $(\boldsymbol{r}, \boldsymbol{\zeta}) \in Q$, where $Q \subset I\!R^2 \times I\!R^3$ is defined in (19). Eq. (15c) defines a mapping $\Phi : Q \to I\!R^2$ from $(\boldsymbol{r}, \boldsymbol{\zeta})$ to the center-of-mass horizontal position $\tilde{\boldsymbol{x}}$ that generates an equilibrium posture. The horizontal cross-section of $\mathcal{R}_{3D}$ is precisely the image of Q under Φ. However, Φ is highly nonlinear and its image is difficult to compute. A natural approximation for the boundary curves of $\widetilde{\mathcal{R}}_{3D}$ is the image of the boundary of Q under Φ. In particular, we are interested in curves on the boundary ∂Q whose projection onto the $\boldsymbol{r}$ plane lies on the boundary of P, while ζ_i lie on the boundary of the friction cones $\mathcal{C}_i$ in the physical space for $i = 1, 2, 3$. The image of these curves under Φ are closed curves in $I\!R^2$, which are taken as an approximation for the boundary of $\widetilde{\mathcal{R}}_{3D}$. The following proposition summarizes the computation of the approximate cross-section $\widetilde{\mathcal{R}}_{3D}$

Proposition 6.4. *A conservative approximation for the region $\widetilde{\mathcal{R}}_{3D}$ is the convex hull of the following curves, each associated with a single edge of the polygonal region P,*

$$\tilde{\boldsymbol{x}}(s) = J \sum_{i=1}^{3} H_i \tilde{f}_i(s) + h_i f_i^z(s) \quad s \in [0, 1], \tag{20}$$

where $\tilde{f}_i(s)$ and $f_i^z(s)$ are computed by composition of the following functions:

$$\begin{aligned}
&\boldsymbol{r}(s) = sv_1 + (1-s)v_2 \\
&\lambda_i(s) = (\boldsymbol{r}(s) - \tilde{x}_{i+1}) \cdot J(\tilde{x}_{i+2} - \tilde{x}_{i+1}) \\
&\zeta_i = \tilde{b}_i^T(\boldsymbol{r}(s) - \tilde{x}_i) \pm \sqrt{(\boldsymbol{r}(s) - \tilde{x}_i)^T \tilde{B}_i (\boldsymbol{r}(s) - \tilde{x}_i)} \\
&\sigma(s) = 1/\left[\textstyle\sum_{i=1}^{3} \lambda_i(s)\zeta_i(s)\right] \\
&\tilde{f}_i(s) = \sigma(s)\lambda_i(s)(\boldsymbol{r}(s) - \tilde{x}_i)\ ,\ f_i^z(s) = \sigma(s)\lambda_i(s)\zeta_i(s),
\end{aligned} \tag{21}$$

where

$$\begin{aligned}
&\tilde{b}_i = -\tfrac{1}{\boldsymbol{e}^T B_i \boldsymbol{e}} E^T B_i \boldsymbol{e} \\
&\tilde{B}_i = \tfrac{1}{(\boldsymbol{e}^T B_i \boldsymbol{e})^2} E^T B_i [(\boldsymbol{e}\boldsymbol{e}^T) - (\boldsymbol{e}^T B_i \boldsymbol{e}) I_{3\times 3}] B_i E \\
&B_i = [s_i \ \ t_i \ \ n_i] \cdot \mathsf{diag}(1, 1, -\mu^2) \cdot [s_i \ \ t_i \ \ n_i]^T
\end{aligned} \tag{22}$$

and v_1, v_2 are two adjacent vertices of the polygonal region P.

Proof: Using Eq. (15c), $\tilde{\boldsymbol{x}}$ can be solved for given $\tilde{f}_i, f_i^z$ as in (20), where $\tilde{f}_i$ and f_i^z are parametrized by $(\boldsymbol{r}, \boldsymbol{\zeta})$ as shown in lemma 6.3. Recall that we compute the image of Φ only for $\boldsymbol{r}$ on the boundary of P, and ζ_i on the boundary of $\mathcal{C}_i$. Hence $\boldsymbol{r}$ is parametrized by a single parameter s as a convex combination of two adjacent vertices v_1 and v_2 of P. Since ζ_i are on the boundary of the friction cone as defined in (19), they must satisfy $(E(\boldsymbol{r} - \tilde{x}_i) + \zeta_i \boldsymbol{e})^T B_i (E(\boldsymbol{r} - \tilde{x}_i) + \zeta_i \boldsymbol{e}) = 0$. (The degenerate case of $\sigma\lambda_i\zeta_i = 0$ occurs when $\vec{f}_i$ vanishes, and only two or less contacts are active.) Solving this quadratic equation for ζ_i gives $\zeta_i(\boldsymbol{r}) = \tilde{b}_i^T(\boldsymbol{r} - \tilde{x}_i) \pm \sqrt{(\boldsymbol{r} - \tilde{x}_i)^T \tilde{B}_i (\boldsymbol{r} - \tilde{x}_i)}$, where $\tilde{b}_i, \tilde{B}_i$ are defined in (22). Composing the parametrization (18) for $\tilde{f}_i$ and f_i^z by $(\boldsymbol{r}, \boldsymbol{\zeta})$ with the parametrization of $\boldsymbol{r}$ and ζ_i by a single parameter s gives the results in (21). Finally, using the convexity of $\widetilde{\mathcal{R}}_{3D}$ (Lemma 6.1), since the curves $\tilde{\boldsymbol{x}}(s)$ lie in $\widetilde{\mathcal{R}}_{3D}$, their convex hull also lies in $\widetilde{\mathcal{R}}_{3D}$. Hence this convex hull gives a conservative approximation for $\widetilde{\mathcal{R}}_{3D}$. □

Example: Figure 12 shows the approximate $\widetilde{\mathcal{R}}_{3D}$ for the 3-contact arrangements depicted in Figure 9. For each contact arrangement the polygonal region P and its vertices were computed, then the boundary curves were computed according to Proposition 6.4, resulting in closed curves. In Figure 12a, the boldface closed loop is the Φ-image of the edge of P connecting the vertices v_1 and v_2. All other curves are associated with other edges of P. The convex hull was then taken by adding tangent segments (dashed lines) which were computed numerically. The result is a convex approximation for $\widetilde{\mathcal{R}}_{3D}$ (shaded region).
The fact that the image of the edges of P do not enclose a convex region is a clear evidence that there are some missing boundary curves, completing the exact boundary of $\widetilde{\mathcal{R}}_{3D}$. These missing boundary curves correspond the image of points $\boldsymbol{r}$ in the *interior* of P. The exact computation of these "interior" curves, and consequently the exact computation of $\widetilde{\mathcal{R}}_{3D}$ is currently under investigation.

7 Concluding Discussion

We have characterized k-contact equilibrium postures in a frictional environment under a planar gravitational field. The feasible equilibrium region of the center-of-mass locations

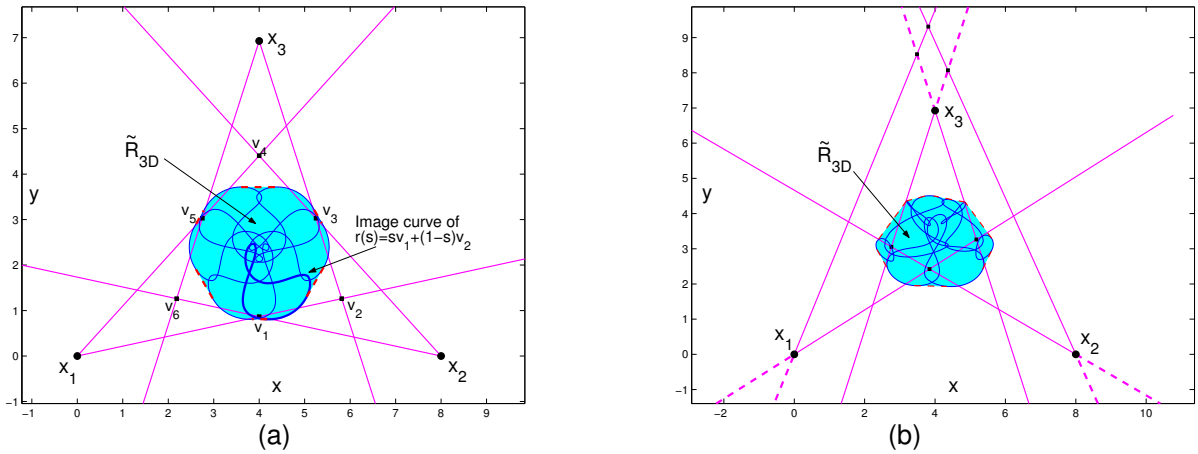

Figure 11: A conservative approximation of $\widetilde{\mathcal{R}}_{3D}$ (shaded) and the boundary curves generated by the edges of the polygon P, for the contact arrangements depicted in Figure 9.

was formulated as a linear programming solution. Additionally, we provided a graphic characterization of this region, presented an efficient geometric algorithm for computing this region, and introduced the notion of essential and redundant contacts. The results were then generalized to guarantee posture's robustness with respect to a neighborhood of disturbance wrenches. Then we extended the results to linear contact patches, and presented preliminary experimental results verifying the theoretical criterion. Finally, we presented first steps towards conservative approximation of feasible equilibrium postures in 3D. We now briefly discuss possible application to quasistatic locomotion planning, and the dynamic analysis of postures' stability.

An important application of the analysis presented in this paper is locomotion planning for multi-limbed robot walking quasistatically on a piecewise linear terrain. The path planning can be reduced to the problem of selecting a sequence of robust equilibrium postures, and suitable transitions between them, which involve quasistatic movement of center-of-mass and free limbs. However, even though this approach seems extremely attractive as a locomotion planner, we must emphasize that the criterion of feasible equilibrium is basically *static*. In order to characterize a suggested posture, one must also consider its *dynamic stability*. For dynamic analysis, one must consider the dynamic response at the contacts under small perturbations, and ensure that the contacts will not break, roll, or slip. A key problem, is that the rigid body dynamics with frictional contacts can be ambiguous [12, 14], and the dynamic analysis must include all possible contact modes [21, 5]. A complete dynamic analysis, where we use the criterion of *strong stability* defined by Trinkle et. al. [20] to characterize robust stable equilibrium postures, will be presented in a paper currently under preperation. The interested reader is referred to [18] for a short paper, and to [19] for a technical report.

References

[1] A. Bicchi. Hands for dexterous manipulation and robust grasping: A difficult road toward simplicity. *IEEE Trans. on Robotics and Automation*, 16(6):652–662, Aug. 2000.

[2] J.-D. Boissonnat, O. Devillers, L. Donati, and F. P. Preparata. Motion planning for spider robots. In *IEEE Int. Conf. on Robotics and Automation*, pages 2321–2326, 1992.

[3] T. Bretl, S. Rock, and J.C. Latombe. Motion planning for a three-limbed climbing robot in vertical natural terrain. In *IEEE Int. Conf. on Robotics and Automation*, pages 2946–2953, 2003.

[4] V. Chvatal. *Linear Programming*. W.H. Freeman and Company, 1983.

[5] M. A. Erdmann. On a representation of friction in configuration space. *The International Journal of Robotics Research*, 13(3):240–271, June 1994.

[6] M. A. Erdmann. An exploration of nonprehensile two-palm manipulation. *The International Journal of Robotics Research*, 17(5), 1998.

[7] F. Fen, M. Shoham, and R. Longman. Lyapunov stability of force-controlled grasps with a multifingered hand. *Int. J. of Robotics Research*, 15(2):137–154, 1996.

[8] W. S. Howard and V. Kumar. On the stability of grasped objects. *IEEE Transactions on Robotics and Automation*, 12(6):904–917, Dec. 1996.

[9] K. L. Johnson. *Contact Mechanics*. Cambridge University Press, 1985.

[10] D. J. Kriegman. Capture regions of curved 3d objects. In *IEEE Int. Conf. on Robotics and Automation*, pages 595–601, 1994.

[11] Q. Lin. Mechanics and planning of workpiece fixturing and robotic grasping. Ph.d. dissertation, Dept. of Mechanical Engineering, 1998, http://robotics.caltech.edu/papers.

[12] P. Lotstedt. Coulomb friction in two-dimensional rigid body systems. *Zeitschrift fur Angewandte Mathematik und Mechanik*, 61:605–615, 1981.

[13] A. Madhani and S. Dubowsky. Motion planning of mobile multi-limb robotic systems subject to force and friction constraints. In *IEEE Int. Conf. on Robotics and Automation*, pages 233–239, 1992.

[14] M. T. Mason and Y. Wang. On the inconsistency of rigid-body frictional planar mechanics. In *IEEE Int. Conf. on Robotics and Aut.*, pages 524–528, 1988.

[15] R. Mason, J. W. Burdick, and E. Rimon. Stable poses of three-dimensional objects. In *IEEE Int. Conf. on Robotics and Automation*, Albuquerque NM, May 1997.

[16] R.B. McGhee and A.A. Frank. On the stability properties of quadruped creeping gaits. *Mathematical Biosciences*, 3(3–4):331–351, 1968.

[17] R. M. Murray, Z. Li, and S. S. Sastry. *A Mathematical Introduction to Robotic Manipulation*. CRC Press, Boca Raton, FA, 1994.

[18] Y. Or and E.Rimon. Robust multiple contact postures in a two-dimensional gravitational field. In *IEEE Int. Conf. on Robotics and Automation*, pages 4783–4788, 2004.

[19] Y. Or and E. Rimon. Robust multiple-contact postures in a two-dimensional gravitational field. Tech. report, Dept. of Mechanical Engineering, Technion, http://robots.technion.ac.il, October 2003.

[20] J. S. Pang and J. C. Trinkle. Stability characterizations of fixtured rigid bodies with coulomb friction. In *IEEE Int. Conference on Robotics and Automation*, pages 361–368, 2000.

[21] V. T. Rajan, R. Burridge, and J. T. Schwartz. Dynamics of rigid body in frictional contact with rigid walls. In *IEEE Int. Conf. on Robotics and Automation*, pages 671–677, 1987.

[22] J. C. Trinkle, , A. O. Farahat, and P. F. Stiller. First-order stability cells of active multi-rigid-body systems. *IEEE Transactions on Robotics and Automation*, 11(4):545–557, Oct 1995.

[23] J. C. Trinkle, A. O. Farahat, and P. F. Stiller. Second-order stability cells of a frictionless rigid body grasped by rigid fingers. In *IEEE Int. Conference on Robotics and Automation*, pages 2815–2821, 1994.

[24] C-H Xiong, Y-F Li, H. Ding, and Y-L Xiong. On the dynamic stability of grasping. *The International Journal of Robotics Research*, 18(9):951–958, 1999.

Appendix - An Algorithm for Computing the 2D Feasible Equilibrium Region for Multiple contacts

We present an algorithm for computing the feasible equilibrium region for a given set of k frictional contacts in a planar gravitational field. For simplicity, we assume the nominal gravitational wrench $\boldsymbol{w}_o = (f_g, 0)$, but the procedure generalizes to any given external wrench.

Notation and terminology:
First, let us define a world frame $\mathcal{F}$ with vertical y-axis and horizontal x-axis, and let $\boldsymbol{e}$ denote the upward pointing unit vector. Recall that each contact point x_i is specified together with the pair (t_i, n_i), denoting the tangent and normal directions at x_i. We now enumerate the infinite directed lines lying on the edges of the friction cones at the contacts, from $-k$ to k as follows:

$$l_j = \{x_{|j|} + s(t_{|j|} + \mu \mathsf{sgn}(j) n_{|j|}) \ , \ s \in I\!R\} \ , \text{ for } j \in \{\pm 1, \ldots, \pm k\},$$

where μ is the coefficient of friction. Each line has the form $l_j = \{(x, y) : y = a_j x + b_j\}$, with (x, y) as the coordinates in $\mathcal{F}$. Hence each line can be parametrized by its slope and intercept (a_j, b_j). We also divide these lines into two groups, left pointing and right pointing with respect to $\boldsymbol{e}$, and define the corresponding index sets as follows:

$$\mathcal{I}_L = \{j : (t_{|j|} + sign(j)\mu n_{|j|}) \cdot J\boldsymbol{e} > 0\} \ , \ \mathcal{I}_R = \{j : (t_{|j|} + sign(j)\mu n_{|j|}) \cdot J\boldsymbol{e} < 0\}.$$

The non-generic case of strictly vertical lines is left for later treatment. It is worth noting that the edges of a particular friction cone can be both left-pointing or both right-pointing (e.g. at x_2 in Figure 7(a)). Recall that we assume that all contacts are upward pointing, in the sense that $(t_i \pm \mu n_i) \cdot \boldsymbol{e} > 0$ for all $i = 1 \ldots k$. Let us define the set $\mathcal{S}$ of all intersection points of left pointing lines with right pointing lines:

$$\mathcal{S} = \{x : x \in l_i \cap l_j \ , \ i \in \mathcal{I}_L \ , \ j \in \mathcal{I}_R\}.$$

Finally, in order to characterize the contacts' geometry, we need the following definitions. Let L be the maximal pairwise distance between the contact points, let α_{max} be the maximal angle of the contact tangents t_i with respect to the horizontal direction, and let δ be the minimal horizontal distance between any two points in $\mathcal{S}$[2]. Recall that the angle of friction is defined as $\gamma = \tan^{-1}(\mu)$, where μ is the coefficient of friction.
A key observation is that the edges of the feasible equilibrium region, $\mathcal{R}(\boldsymbol{w}_o)$, are vertical lines that pass through points of $\mathcal{S}$. Furthermore, the right edge of $\mathcal{R}(\boldsymbol{w}_o)$ passes through the *rightmost* point of $\mathcal{S}$, and the left edge of $\mathcal{R}(\boldsymbol{w}_o)$ passes through the *leftmost* point in $\mathcal{S}$. The problem of computing $\mathcal{R}(\boldsymbol{w}_o)$ therefore reduces to finding the points of $\mathcal{S}$ with maximal and minimal x-coordinate. The naive computation requires inspection of all k^2 points of $\mathcal{S}$. The efficient algorithm presented below (inspired by the *Line Sweep* algorithm) is essentially *linear* in k.

[2]More precisely, $\delta = min\{\delta_L, \delta_R\}$, where δ_L is the horizontal distance between the two leftmost points in $\mathcal{S}$, and δ_R is the horizontal distance between the two rightmost points in $\mathcal{S}$.

Algorithm description:
First we give a high-level description of the algorithm. For simplicity, we only describe how to compute the right edge of $\mathcal{R}(\boldsymbol{w}_o)$, while the left edge is computed similarly. In the initialization stage, we choose a vertical line $x = x_R$, which is guaranteed to lie *outside* $\mathcal{R}(\boldsymbol{w}_o)$ on its right side, and another vertical line $x = x_L$, which passes through a point of $\mathcal{S}$ (Figure 7(a)). The intersection point of all lines l_j with the vertical line $x = x_R$ is given by $y_j = a_j x_R + b_j$. A key fact is that the line $x = x_R$ satisfies a separation condition, in the sense that the intersection point of any right-pointing line with $x = x_R$ lies *above* the intersection point of any left-pointing line with $x = x_R$ (Figure 7(a)).[3] On the other hand, this separation does not occur on the line $x = x_L$. A critical separation condition is satisfied on the right edge of $\mathcal{R}(\boldsymbol{w}_o)$: it is the vertical line on which the lowest intersection of right-pointing lines and the highest intersection of left-pointing lines coincide. It is the line labelled $x = x'_L$ in Figure 7(a). The main loop of the algorithm consists of three steps that systematically increase x_L and decrease x_R, until the line $x = x_L$ satisfies the critical separation condition. The three steps are as follows.
First, the segment $[x_L, x_R]$ is bisected at its midpoint, which is denoted x_m. Then the intersection point of each line l_j with the vertical line $x = x_m$ is computed. If the line $x = x_m$ satisfies the separation condition x_R is replaced by x_m, and otherwise x_L is replaced by x_m. Second, the intersection point of each line l_j with the line $x = x_L$ is computed. Let p_L denote the highest intersection point of a left-pointing line with $x = x_L$, and let p_R denote the lowest intersection point of a right-pointing line with $x = x_L$ (Figure 7(a)). Any right-pointing line whose intersection with $x = x_L$ lies above or at p_L, is redundant, in the sense that it has no intersection with left-pointing lines on the right side of $x = x_L$. Therefore, such lines are deleted by removing their indices from $\mathcal{I}_R$. Similarly, any left-pointing line whose intersection with $x = x_L$ lies below or at p_R is deleted. In the example of Figure 7(a), the left-pointing line l_{-1} is redundant, since it intersects the line $x = x_L$ below p_R, while none of the right-pointing lines is redundant. Third, the algorithm selects the right-pointing line l_R corresponding to p_R, and moves the line $x = x_L$ to pass through the rightmost intersection point of left-pointing lines in $\mathcal{I}_L$ with l_R. In the example of Figure 7(a), the right-pointing line corresponding to p_R is l_3. It intersects the non-redundant left-pointing lines l_{-2}, l_{-3} and l_2. The rightmost intersection occurs with l_{-3}, and the line $x = x_L$ is moved to pass through that point. The new line is labelled $x = x'_L$ in Figure 7(a). This choice gives a new location for the line $x = x_L$ which passes through a new point of $\mathcal{S}$, located to the right of the previous one. Moreover, this choice guarantees that in the next step, the right-pointing line l_R automatically becomes redundant since it passes through the new p_L.
The three steps are executed repeatedly, until $x = x_L$ satisfies the critical separation condition. At this stage, all the lines become redundant, the index sets $\mathcal{I}_L$ and $\mathcal{I}_R$ become empty, and the algorithm terminates with $x = x_L$ as the output.

[3]Note that since we assumed that all lines are upward pointing, the left pointing lines must have negative slopes, and the right pointing lines must have positive slopes.

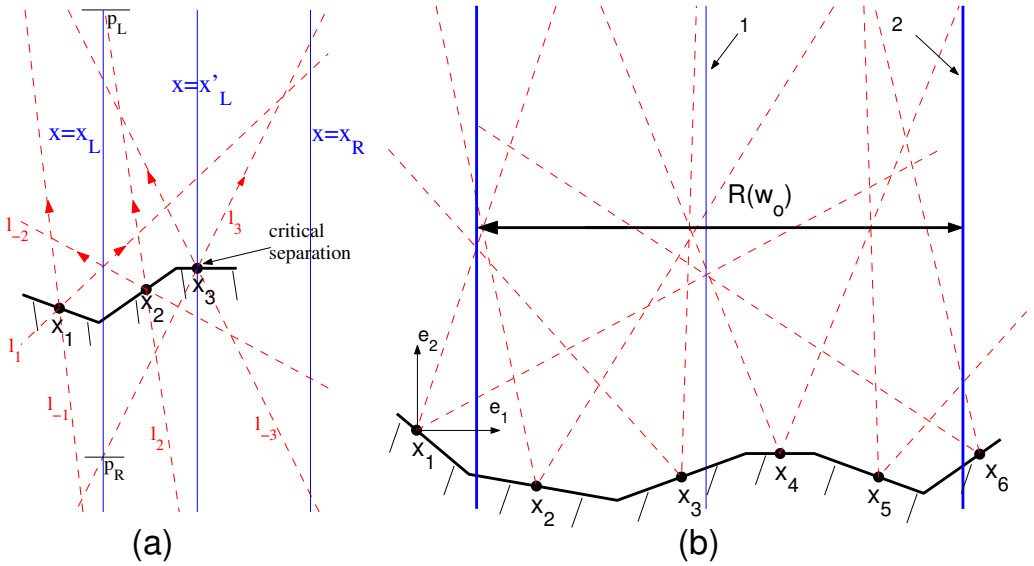

Figure 12: (a) An Illustrative example of a single step execution.
(b) A Full execution example for six contacts with $\mu = 0.4$.

Algorithm $\mathcal{R}(\boldsymbol{w}_o) - 2D$

1. Initializations

Set $a_{Lmax} = \max_{j \in \mathcal{I}_L} a_j$, and set $a_{Lmin} = \min_{j \in \mathcal{I}_L} a_j$.
Set $a_{Rmax} = \max_{i \in \mathcal{I}_R} a_i$, and set $a_{Rmin} = \min_{i \in \mathcal{I}_R} a_i$.
Set $b_{Lmax} = \max_{j \in \mathcal{I}_L} b_j$, and set $b_{Rmin} = \min_{i \in \mathcal{I}_R} b_i$.
Set $x_R = \max\{\frac{b_{Lmax} - b_{Rmin}}{a_{Rmin} - a_{Lmax}}, \frac{b_{Lmax} - b_{Rmin}}{a_{Rmax} - a_{Lmin}}\}$.
Set $i_R = \arg\min_{i \in \mathcal{I}_R} a_i x_R + b_i$, and set $j_L = \arg\max_{j \in \mathcal{I}_L} a_j x_R + b_j$.
Set $x_L = \frac{b_{j_L} - b_{i_R}}{a_{i_R} - a_{j_L}}$.
If $x_L = x_R$, return $x = x_R$ and STOP.

2. Repeat:

2.1 Set $x_m = \frac{x_L + x_R}{2}$.
2.2 Set $y_{Lmax} = \max_{j \in \mathcal{I}_L} a_j x_m + b_j$
2.3 Set $y_{Rmin} = \min_{i \in \mathcal{I}_R} a_i x_m + b_i$
2.4 If $y_{Rmin} \leq y_{Lmax}$ set $x_L = x_m$, and goto step 2.7. Else, set $x_R = x_m$.
2.5 Set $y_{Lmax} = \max_{j \in \mathcal{I}_L} a_j x_L + b_j$.
2.6 Set $y_{Rmin} = \min_{i \in \mathcal{I}_R} a_i x_L + b_i$.
2.7 Remove from $\mathcal{I}_R$ any i such that $a_i x_L + b_i \geq y_{Lmax}$.
2.7 Remove from $\mathcal{I}_L$ any j such that $a_j x_L + b_j \leq y_{Rmin}$.
2.9 If $\mathcal{I}_R$ or $\mathcal{I}_L$ becomes empty return $x = x_L$ and STOP.
2.10 Set $i_R = \arg\min_{i \in \mathcal{I}_R} a_i x_L + b_i$.
2.11 Set $x_L = \max_{j \in \mathcal{I}_L} \frac{b_j - b_{i_R}}{a_{i_R} - a_j}$.
(* End of repeat loop *)

The correctness and run time of the algorithm is summarized in the following lemma.

Lemma 7.1. *For a gravitational wrench $\boldsymbol{w}_o = (f_g, 0)$ and a given set of k frictional contacts, the algorithm $\mathcal{R}(\boldsymbol{w}_o) - 2D$ terminates and returns the right edge of the feasible equilibrium region $\mathcal{R}(\boldsymbol{w}_o)$. Furthermore, the algorithm runs in $O(k \cdot \min\{k, \log(\Delta/\delta)\})$ steps, where $\Delta = L\frac{1+\tan(\alpha_{max}+\gamma)}{\cot(\alpha_{max}+\gamma)}$, and $\gamma, \delta, L, \alpha_{max}$ are geometric constants defined above.*

Proof: In the initialization stage, the algorithm chooses a vertical line, $x = x_L$, which passes through a point of $\mathcal{S}$. At the end of each iteration of the main loop, the line $x = x_L$ moves to the right and passes through a new point of $\mathcal{S}$. Since the x-coordinate of the intersection point of two lines l_i and l_j is given by $x = \frac{b_i - b_j}{a_j - a_i}$, the choice of x_R guarantees that no point of $\mathcal{S}$ lies to the right of the line $x = x_R$, and hence it satisfies the separation condition.

In steps 2.5-2.8, some lines are deleted, and their indices are removed from the sets $\mathcal{I}_L$ and $\mathcal{I}_R$. The sets $\mathcal{I}_L$ and $\mathcal{I}_R$ are empty if and only if the line $x = x_L$ satisfies the critical separation condition, and passes through the *rightmost* point of $\mathcal{S}$. Therefore, the algorithm returns the right edge of $\mathcal{R}(\boldsymbol{w}_o)$.

We now show that at each iteration, at least one line is deleted. In step 2.11, let us define $j_L = \arg\max_{j \in \mathcal{I}_L} \frac{b_j - b_{i_R}}{a_{i_R} - a_j}$. Using the definition of x_L in step 2.11, one gets:

$$x_L = \frac{b_{j_L} - b_{i_R}}{a_{i_R} - a_{j_L}} \geq \frac{b_j - b_{i_R}}{a_{i_R} - a_j} \text{ , for all } j \in \mathcal{I}_L.$$

Recall that $a_{i_R} - a_j > 0$ for all $i_R \in \mathcal{I}_R$ and $j \in \mathcal{I}_L$. Substituting x_L and using simple algebraic manipulations, one can get:

$$a_{j_L} x_L + b_{j_L} \geq a_j x_L + b_j \text{ , for all } j \in \mathcal{I}_L.$$

Therefore, in the next execution of step 2.5, we get that $y_{Lmax} = a_{j_L} x_L + b_{j_L}$. Since l_{i_R} and l_{j_L} intersect at $x = x_L$, we also get that $y_{Lmax} = a_{i_R} x_L + b_{i_R}$, and hence i_R is removed from $\mathcal{I}_R$ in step 2.7.

Let us now verify the algorithm's run time. The initialization stage requires going over all lines, and hence takes $O(k)$ time. A single iteration of the main loop also takes $O(k)$ time. Since at least one line is deleted at each iteration, the algorithm stops after at most $O(k)$ iterations. Furthermore, the length of the segment $[x_L, x_R]$ decreases by at least *one half* in each iteration. When $X_R - x_L < \delta$, only the rightmost point of $\mathcal{S}$ still lies between $x = x_L$ and $x = x_R$, and it will be discovered in step 2.11. Hence the number of iterations is bounded by $O(\log \frac{\Delta_o}{\delta})$, where Δ_o equals $x_R - x_L$ after the initialization stage. Recall that $\gamma = \tan^{-1}(\mu)$ is the half-angle of the friction cones. Since the lowest angle of lines l_j about the horizontal direction is $90^o - (\alpha_{max} + \gamma)$, it can be shown using geometric relations that $\Delta_o \leq L\frac{1+\tan(\alpha_{max}+\gamma)}{\cot(\alpha_{max}+\gamma)}$. Hence the overall time complexity is $O(k \cdot \min\{k, \log(\Delta/\delta)\})$, where $\Delta = L\frac{1+\tan(\alpha_{max}+\gamma)}{\cot(\alpha_{max}+\gamma)}$. □

In a worst case scenario the algorithm is $O(k^2)$, which is the same as a straightforward computation of all points in $\mathcal{S}$. However, the algorithm significantly reduces the number of active lines at each iteration, and is therefore significantly more efficient. Furthermore, for any practical set of contacts, the quantity $\log(\Delta/\delta)$ is a small constant. Therefore, the time complexity of the algorithm is practically linear in k. Finally, in the special case where there exists a vertical line $l_j = \{(x, y) : x = x_o\}$, we only need to add the following simple check after step 2.11:

If $x_L \geq x_o$, return $x = x_o$ and STOP.

Execution Example:
Consider an application of the algorithm for a posture of six frictional contacts with $\mu = 0.4$ shown in Figure 7(a). The fixed frame origin is positioned at x_1. When computing the right edge of $\mathcal{R}(\boldsymbol{w}_o)$, the line labelled '1' is the initial $x = x_L$ line. The line labelled '2' is $x = x_L$ after the first execution of the main loop, and then the algorithm stops. Note that the naive computation requires inspection of $6^2 = 36$ intersection points!